Piezoresponse Force Microscopy with Asylum Research AFMs

Asylum Research

Roger Proksch, Asylum Research and Sergei Kalinin, Center for Nanophase Materials Sciences (CNMS) at Oak Ridge National Laboratory

Introduction

Electromechanical coupling is one of the fundamental mechanisms underlying the functionality of many materials. These include inorganic macro-molecular materials, such as piezo- and ferroelectrics, as well as many biological systems. This application note discusses the background, techniques, problems and solutions to piezoresponse force microscopy (PFM) measurements using the **MFP-3D**™ and **Cypher**™ AFMs from Asylum Research.

Background

The functionality of systems ranging from non-volatile computer memories and micro electromechanical systems to electromotor proteins and cellular membranes are ultimately based on the intricate coupling between electrical and mechanical phenomena.[1] The applications of electromechanically active materials include sonar, ultrasonic and medical imaging, sensors, actuators, and energy harvesting technologies. In the realm of electronic devices, piezoelectrics are used as components of RF filters and surface-acoustic wave (SAW) devices.[2] The ability of ferroelectric materials to switch polarization orientation – and maintain polarization state in a zero electric field – has lead to emergence of concepts of non-volatile ferroelectric memories and data storage devices.[3] Electromechanical coupling is the basis of many biological systems, from hearing to cardiac activity. The future will undoubtedly see the emergence, first in research labs and later in industrial settings, of the broad arrays of piezoelectric, biological and molecular-based electromechanical systems. Progress along this path requires the ability to image and quantify electromechanical functionalities on the nanometer and molecular scale (Figures 1 and 2). Areas such as nanomechanics and single-molecule imaging and force measurements have been enabled by the emergence of microscopic tools such as nanoindentation and protein unfolding spectroscopy.

Similarly, the necessity for probing electromechanical functionalities has led to the development of PFM as a tool for local nanoscale imaging, spectroscopy, and manipulation of piezoelectric and ferroelectric materials.[4]

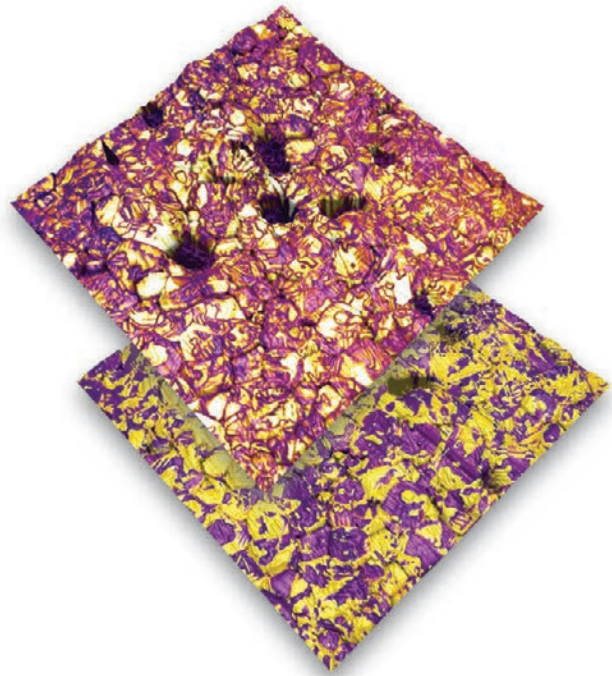

Figure 1: PFM amplitude channel overlaid on AFM height (top) and phase image overlaid on height (bottom) of lead zirconium titanate (PZT), 20 µm scan.

Principles of PFM

1. Basics

PFM measures the mechanical response when an electrical voltage is applied to the sample surface with a conductive tip of an AFM. In response to the electrical stimulus, the sample then locally expands or contracts as shown in Figure 3.

When the tip is in contact with the surface and the local piezoelectric response is detected as the first harmonic component of the tip deflection, the phase φ, of the electromechanical response of the surface yields information on the polarization direction below the tip. For c- domains (polarization vector oriented normal to the surface and pointing downward), the application of a positive tip bias results in the expansion of the sample, and surface oscillations are in phase with the tip voltage, $\varphi = 0$. For c+ domains,

OXFORD INSTRUMENTS
The Business of Science®

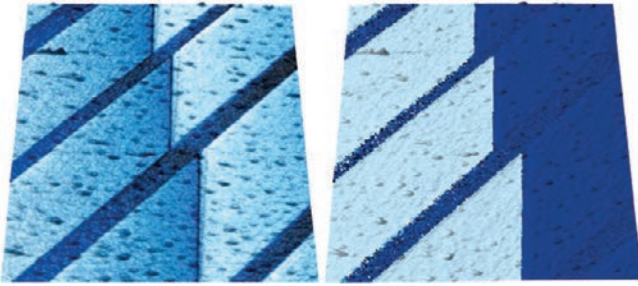

Figure 2: PFM amplitude overlaid on AFM topography (left) and PFM phase overlaid on topography (right) on (100) oriented $BaTiO_3$ single crystal (from Castech Crystals). The amplitude and phase image show 90° and 180° domain walls in $BaTiO_3$. 10 μm scan courtesy of V.R. Aravind, K. Seal, S. Kalinin, ORNL, and V. Gopalan, Pennsylvania State University.

the response is opposite and $\varphi = 180°$. More details are given in Section 2 (below).

Detection of the lateral components of tip vibrations provides information on the in-plane surface displacement, known as lateral PFM. A third component of the displacement vector can be determined by imaging the same region of the sample after rotation by 90°.[5] Provided that the vertical and lateral PFM signals are properly calibrated, the complete electromechanical response vector can be determined, an approach referred to as vector PFM.[6] Finally, electromechanical response can be probed as a function of DC bias of the tip, providing information on polarization switching in ferroelectrics, as well as more complex electrochemical and electrocapillary processes.[7,8]

PFM requires detection of small tip displacements induced by relatively high amplitude, high frequency voltages measured at the same frequency as the drive. Any instrumental crosstalk between the drive and the response will result in a virtual PFM background that can easily be larger than the PFM response itself, especially for weak piezo materials. Minimizing crosstalk between the driving voltage and the response imposes a number of serious engineering limitations on the microscope mechanics and electronics. In the past, significant post-factory modifications were required to decouple the drive and response signals. Asylum's PFM uses a unique proprietary design of the head and the high voltage sample holder to eliminate drive crosstalk (see page 10).

2. Piezo Effect

The relationship between the strain and the applied electric field (often referred to as the "inverse piezo effect") in piezoelectric materials is described by a rank-3 tensor. The most important component of this tensor for typical "vertical" PFM is the d_{33} component,[9] since it couples directly into the vertical motion of the cantilever. The voltage applied to the tip is:

$$V_{tip} = V_{dc} + V_{ac} \cos(\omega t), \quad (1)$$

resulting in piezoelectric strain in the material that causes cantilever displacement:

$$z = z_{dc} + A(\omega, V_{ac}, V_{dc}) \cos(\omega t + \varphi) \quad (2)$$

due to piezoelectric effect.[10] When the voltage is driven at a frequency well below that of the contact resonance of the cantilever, this expression becomes:

$$z = d_{33} V_{dc} + d_{33} V_{ac} \cos(\omega t + \varphi), \quad (3)$$

where we have implicitly assumed depends on the polarization state of the material. From this last equation and from Figure 3, the magnitude of the oscillating response is a measure of the magnitude of d_{33} and the phase is sensitive to the polarization direction of the sample.

NOTE: In reality, the d_{33} component in Equation 3 is an "effective" d_{33} that depends on the contribution from other tensor elements and on the crystallographic and real space orientation of the piezo material, as well as details of the tip-sample contact.

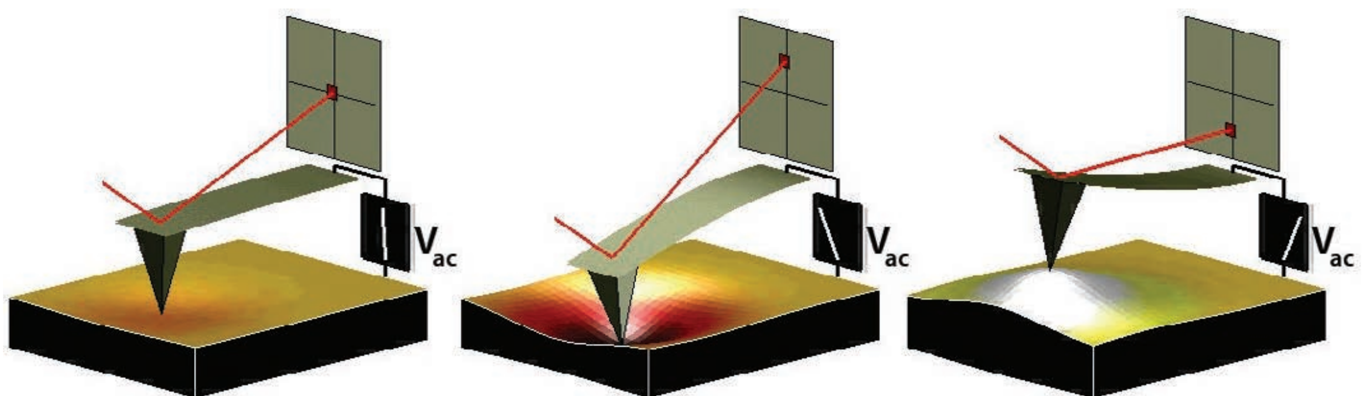

Figure 3: Depiction of PFM operation. The sample deforms in response to the applied voltage. This, in turn, causes the cantilever to deflect, which can then be measured and interpreted in terms of the piezoelectric properties of the sample. Image courtesy S. Jesse, ORNL.

Table 1

Material	Application	d_{33},pm/V note 1	Coercive bias (for local switching) note 2	Breakdown voltage/onset of conductivity note 3
Bulk Materials				
PZT ceramics	Actuators & transducers	100-500	10 V - 1 kV	N/A
$LiNbO_3$ single crystals	Electro-optical devices	10-20	10 V - 1 kV	N/A
Quartz	Balances, frequency standards	3	N/A	N/A
Polar semiconductors	RF devices, switches	0.1-2	N/A	
Calcified tissues		0.5-3	N/A	N/A
Collagen		0.5-3	N/A	N/A
Thin Films and Capacitor Structures				
1-5 micron PZT	Capacitors	10-30	1-100	100
~100-300 nm PZT	FeRAM elements	3-10	1-10	10-20
30-100 nm $BiFeO_3$	FeRAM	3-10	1-10	10-20
Ultrathin Films				
1-5 nm $BiFeO_3$	Tunneling barriers	1-10	1-5	10 (can be below switching voltage in air)
10 nm PVDF	Actuators	20	2-5	10

**1. The PFM signal is given by Equation 6, $A = d_{33}$ Vac Q where d_{33} is material property, V_{ac} is driving voltage, and Q is the quality factor. Q = 1 for low frequency PFM, and Q = 20-100 if resonance enhancement (DART or BE) method is used. V_{ac} is limited by material stability and polarization switching. The microscope photodetector sensitivity, thermal noise and shot noise impose the limit A > 30 pm. The ultimate limit is A = thermal noise.*

**2. Quantitative spectroscopic measurements require probing bias to be one to two orders of magnitude smaller than coercive bias, limiting the voltage amplitude.*

**3. Measurements are not possible above this limit due to sample and tip degradation.*

Typical values for range from 0.1 pm/V for weak piezo materials to 500 pm/V for the strongest. Table 1 shows a listing of representative values.

As mentioned above, the direction of sample polarization determines the sign of the response. Figure 4 demonstrates this idea. If the polarization is parallel and aligned with the applied electric field, the piezo effect will be positive, and the sample will locally expand. If the local sample polarization is anti-parallel with the applied electric field, the sample will locally shrink. This sign-dependent behavior means that the phase of the cantilever provides an indication of the polarization orientation of the sample when an oscillating voltage is applied to the sample.

The relationship in Equation 1 and the values for in Table 1 suggest that typical deflections for a PFM cantilever are on the order of picometers. While the sensitivity of AFM cantilevers is quite impressive – of the order of a fraction of an angstrom (or tens of pm) in a 1 kHz bandwidth – it also implies a very small signal-to-noise ratio (SNR) for all but the strongest piezo materials.

Because of this small SNR, piezoelectricity is most frequently detected by a lock-in amplifier connected to the deflection of the AFM cantilever. By employing an oscillating electric field, low-frequency noise and drift can be eliminated from the measurement. Until recently, PFM was usually accomplished by researchers who modified a commercial SPM system with an external function generator/lock in setup. As a result, in most cases, the operation frequency was limited to <100 kHz. This and the lack of sophisticated control options precluded the use of resonance enhancement (see sections below on DART and BE) in PFM since typical contact resonance frequencies are >300 kHz.

Piezoresponse Force Microscopy with Asylum Research AFMs

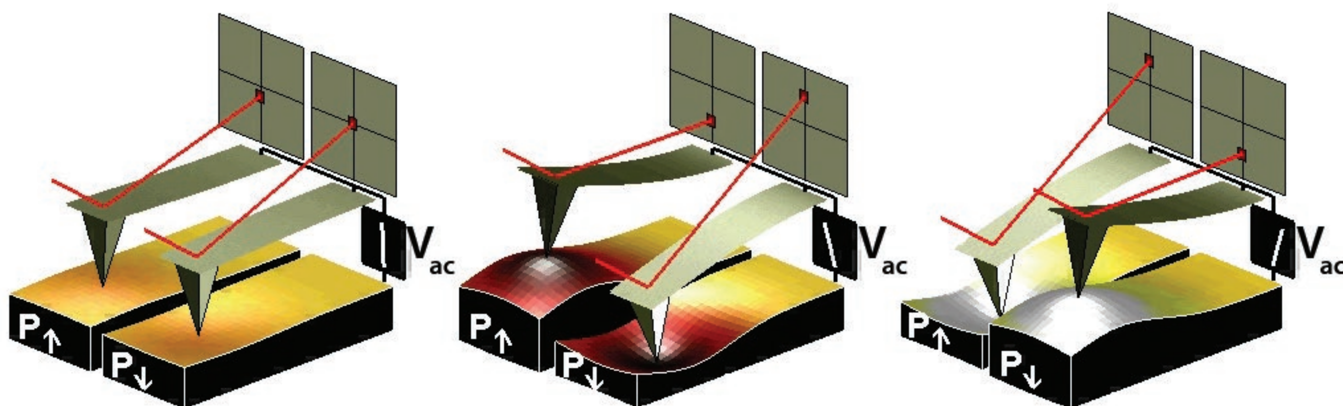

Figure 4: Sign dependence of the sample strain. When the domains have a vertical polarization that is pointed downwards and a positive voltage is applied to the tip, the sample will locally expand. If the polarization is pointed up, the sample will locally contract. The phase of the measured response is thus proportional to the direction of the domain polarization. Figure courtesy of S. Jesse, ORNL.

3. PFM Imaging Modes

The three typical PFM imaging modes and piezoelectric lithography are briefly described below.

A. Vertical PFM

In vertical PFM imaging, out-of-plane polarization is measured by recording the tip-deflection signal at the frequency of modulation. Figure 5 shows an example image of vertical PFM for a lead titanate film. Antiparallel domains with out-of-plane polarization can be seen in the PFM phase image, while in-plane domains are seen in the PFM amplitude image as yellow stripes due to the weak vertical piezoresponse signal

B. Lateral PFM

Lateral PFM is a technique where the in-plane component of polarization is detected as lateral motion of the cantilever due to bias-induced surface shearing. Eng et al.,[11,12] Abplanalp et al.,[13] and Eng et al.,[14] have recently shown that the in-plane component of the polarization can be observed by following the lateral deflection of the AFM cantilever, and have applied this technique to reconstruct the three-dimensional distribution of polarization within domains of ferroelectric single crystals. Roelofs et al. applied this method in order to differentiate 90° and 180° domain switching in $PbTiO_3$ thin films.[15]

C. Vector PFM

In vector PFM, the real space reconstruction of polarization orientation comes from three components of piezoresponse: vertical PFM plus at least two orthogonal lateral PFM.[6] Figure 6 shows an example of a vector PFM image of a barium strontium titanate film (BST), permitting qualitative inspection of the correlation of grain size, shape and location with local polarization orientation and domain wall character. Here, the color wheel permits identification of the local orientation of the polarization. Regions colored as cyan (darker blue/green) possess polarizations which are oriented predominantly normal to the plane of the film, whereas regions that appear magenta-blue or light green possess polarizations which are oriented predominantly within the plane of the film. The intensity of the color map denotes the magnitude of the response.

D. Lithography

For ferroelectric applications, PFM can be used to modify the ferroelectric polarization of the sample through the application of a bias. When the applied field is large enough (e.g. greater than the local coercive field) it can induce ferroelectric polarization reversal. This technique can be used to ‘write’ single domains, domain arrays, and complex patterns without changing the surface topography. Figure 7 shows an example

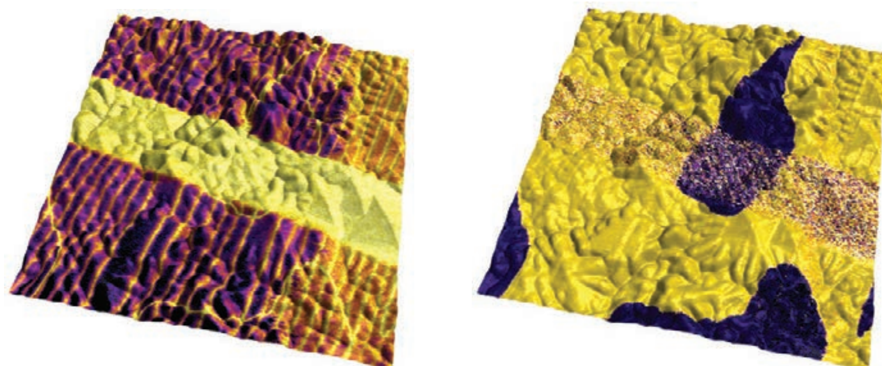

Figure 5: Vertical PFM amplitude overlaid on AFM topography (left) and PFM phase overlaid on AFM topography (right) images of lead titanate film, 5 µm scan. Images courtesy of A. Gruverman and D. Wu, UNL. Sample courtesy H. Funakubo.

of PFM bit-mapped lithography where the color scale of a black and white photo was used to control the bias voltage of the tip as it rastered over the surface and then re-imaged in PFM mode.

4. Spectroscopy Modes

PFM spectroscopy refers to locally generating hysteresis loops in ferroelectric materials. From these hysteresis loops, information on local ferroelectric behavior such as imprint, local work of switching, and nucleation biases can be obtained.

Understanding the switching behavior in ferroelectrics on the nanometer scale is directly relevant to the development and optimization of applications such as ferro-electric non-volatile random access memory (FRAM), and high-density data storage. Multiple studies have addressed the role of defects and grain boundaries on domain nucleation and growth, domain wall pinning, illumination effects on the built-in potential, and domain behavior during fatigue.[15] The origins of the field date back to the seminal work by Landauer, who demonstrated that the experimentally observed switching fields correspond to impossibly large (~10^3 - 10^5 kT) values for the nucleation activation energy in polarization switching. Resolving this 'Landauer paradox' requires the presence of discrete switching centers that initiate low-field nucleation and control macroscopic polarization switching.[16] However, difficulties related to positioning of the tip at a specific location on the surface (due in part to microscope drift), as well as time constraints related to hysteresis loop acquisition, limit these studies to only a few points on the sample surface, thus precluding correlation between the material's microstructure and local switching characteristics.

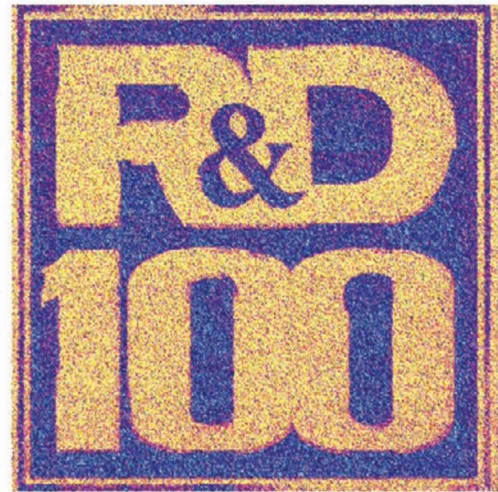

Figure 7: R&D 100 logo written on a sol-gel PZT thin film by PFM lithography. PFM phase is overlaid on top of the rendered topography, 25 µm scan. Oak Ridge and Asylum Research were awarded an R&D100 award for Band Excitation in 2008.

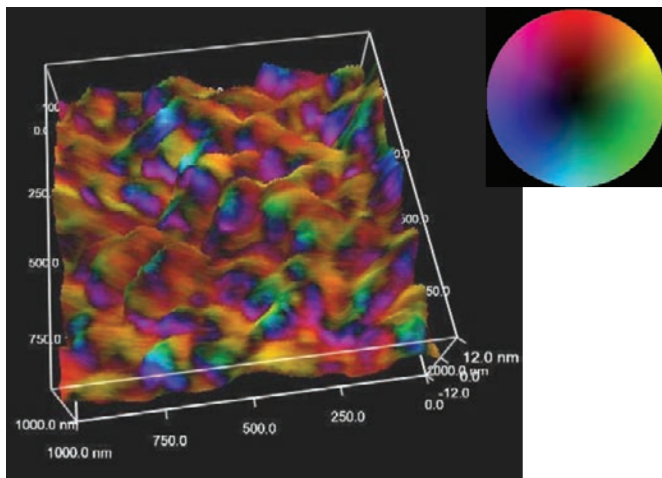

Figure 6: BST film with vector PFM overlaid on AFM topography, 1 µm scan. Image courtesy of C. Weiss and P. Alpay, Univ. of Conn., and O. Leaffer, J. Spanier, and S. Nonnenmann, Drexel University. Color wheel indicates PFM vector orientation.

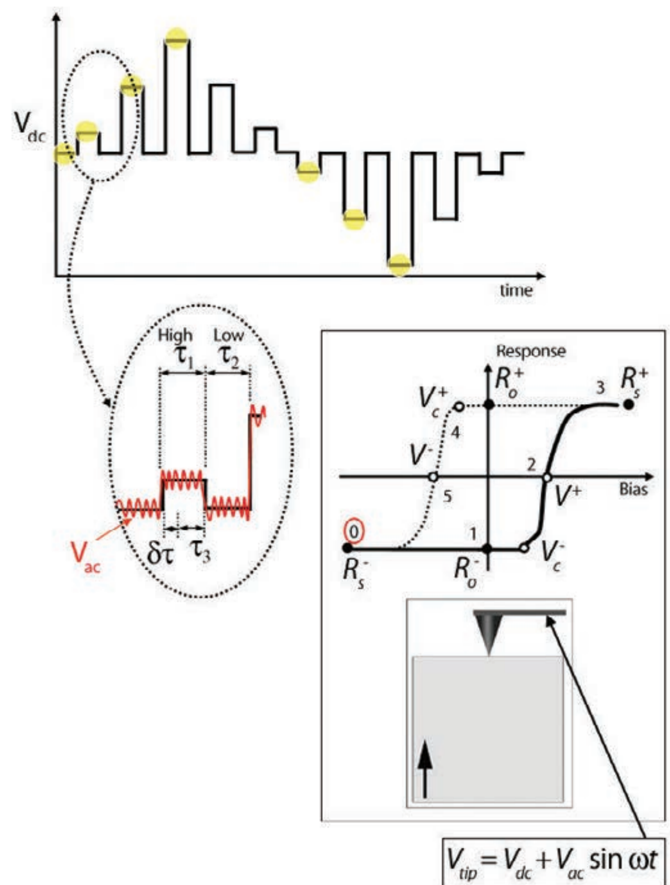

Figure 8: Switching spectroscopy PFM diagram (see text for discussion). Reused with permission from Jesse, Baddorf, and Kalinin, Applied Physics Letters ***88****, 062908 (2006). Copyright 2006, American Institute of Physics.*

A. Switching Spectroscopy Mapping

A new spectroscopy technique, Switching Spectroscopy PFM (SS-PFM), has demonstrated real-space imaging of the energy distribution of nucleation centres in ferroelectrics, thus resolving the structural origins of the Landauer paradox.[17] These maps can be readily correlated with surface topography or other microscopic techniques to provide relationships between micro- and nanostructures and local switching behavior of ferroelectric materials and nanostructures. Figure 8 shows how it works. In SS-PFM, a sine wave is carried by a square wave that steps in magnitude with time. Between each ever-increasing voltage step, the offset is stepped back to zero with the AC bias still applied to determine the bias-induced change in polarization distribution (e.g. the size of the switched domain). It is then possible to see the hysteresis curve of the switching of the polarization of the surface (bottom diagram). If the measurements are performed over a rectangular grid, a map of the switching spectra of that surface can be obtained. Figure 9 shows an example image of a $LiNbO_3$ sample with the PFM signal overlaid on top. The image was taken after switching spectroscopy. The graph shows the hysteresis loops measured at one individual point.

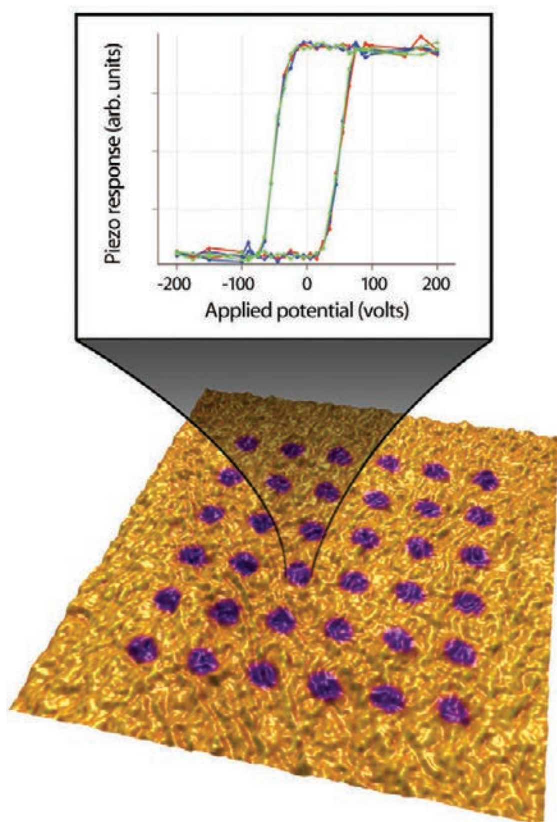

Figure 9: Rendered topography of a $LiNbO_3$ sample with the PFM signal overlaid on top, 4 μm scan.

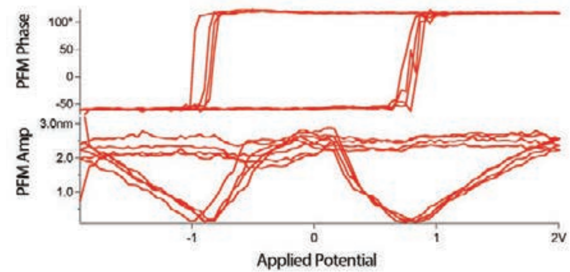

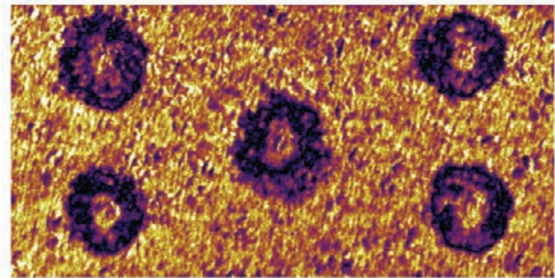

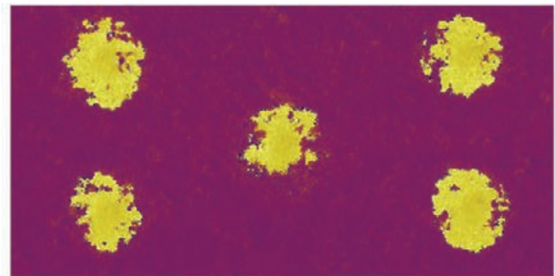

Figure 10: Sol gel PZT sample where local hysteresis loops were measured and displayed (representative phase and amplitude loops shown at top). After the switching spectroscopy measurements, the area was imaged, the DART amplitude (middle) and phase (bottom) are shown, 3.5 μm scan.

As additional examples, Figure 10 shows a sol gel PZT sample where the local switching fields were measured. After the switching spectroscopy, the area was re-imaged. The PFM signal clearly shows five dots in the phase signal denoting portions of the sample where the polarization was reversed during the hysteresis measurements. Figure 11 shows SSM-PFM of capacitor structures and Figure 12 shows an image of phase and amplitude hysteresis loops measured at five different locations on a lead zinc niobate - lead titanate (PZN-PTi) thin film.

Limitations of Conventional PFM Methodologies

1. High Voltage Limitations

Traditionally, the use of 1-10 Vpp driving amplitude on materials with strong electromechanical responses (e.g. $d_{33} \approx 500$ pm/V for PZT, 10 pm/V for $LiNbO_3$) allowed direct imaging and spectroscopy of ferroelectric materials sufficient for applications corresponding to a detection limit of 50 pm at ~100 kHz.

Measurements of lower sensitivity materials require the use of higher voltages or the use of contact resonance.

2. Imaging at Contact Resonance

For some samples, using a higher drive voltage is undesirable. High drive voltages will result in polarization switching or even damage to the sample. Recent advances in theoretical understanding of the PFM imaging mechanism illustrate that the primary limitation of previous commercial and home built SPMs is their inability to effectively use resonance enhancement.

Probe polarization dynamics in commercial low voltage ferroelectric capacitors is optimal for driving amplitudes of 30-100 mV (to avoid bias-induced changes in domain structures), which is 1-2x below the magnitude of standard, low-frequency PFM capabilities. Finally, the use of PFM as an electrophysiological tool necessitates operation in the mV regime, as required to prevent damage to biological systems, as well as stray electrochemical reactions.[18]

The resonant frequencies are determined only by the weakly voltage-dependent mechanical properties of the system and are independent of the relative contributions of the electrostatic and electromechanical interactions. As shown by Sader[19] in the vicinity of a resonance for small damping ($Q > 10$), the amplitude and phase frequency response can be described using the harmonic oscillator model[20] as:

$$A(\omega) = \frac{A_{max}\omega_0^2/Q}{\sqrt{\left(\omega_0^2-\omega^2\right)^2+\left(\omega_0\omega/Q\right)^2}} \qquad (4)$$

$$\tan\varphi(\omega) = \frac{\omega_0\omega}{Q\left(\omega_0^2-\omega^2\right)} \qquad (5)$$

where, A_{max} is the amplitude at the resonance ω_0, and Q and is the quality factor that describes energy losses in the system. Resonance is a phenomenon used in many SPM techniques. The cantilever response at resonance is essentially multiplied by the so-called "quality factor" (Q) of the cantilever:

$$A = d_{33} V_{ac} Q \qquad (6)$$

Typical Q values in air for PFM cantilevers range from 10-100x. This implies that one can amplify a weak PFM signal by a factor of 10-100x by simply driving the tip voltage at the contact resonant frequency.

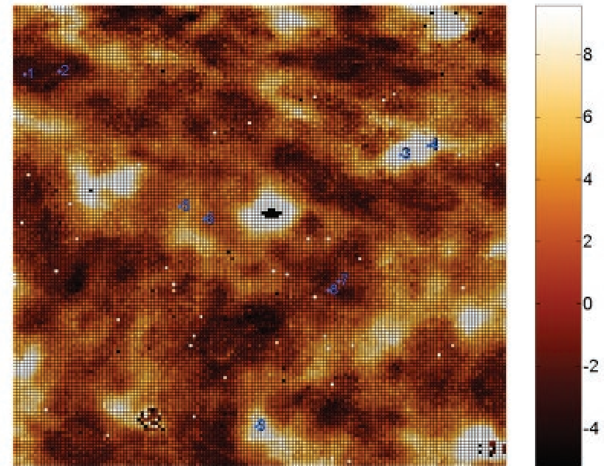

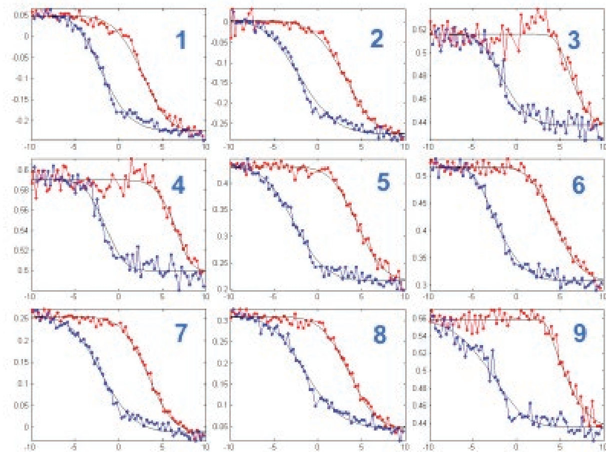

Figure 11: SS-PFM and hysteresis loops of capacitor structures. Data courtesy K. Seal and S.V. Kalinin, ORNL. Sample courtesy P. Bintacchit and S. Trolier-McKinstry, Penn State Univ.

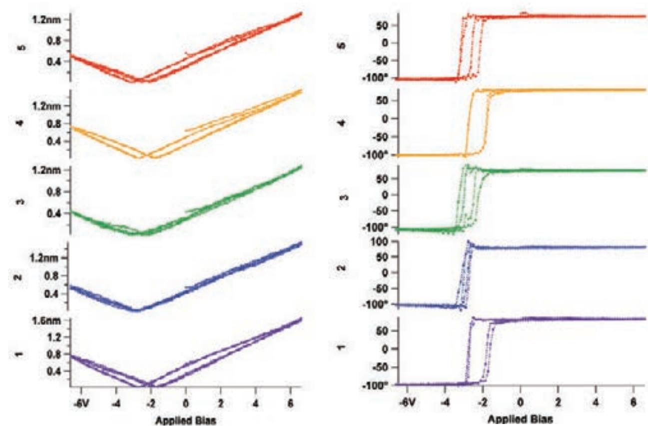

Figure 12: Amplitude (left) and phase (right) hysteresis loops measured at five different locations on a PZN-PTi thin film.

Figure 13 shows a representative cantilever in contact with a surface. The potential of the cantilever is being oscillated, which in turn induces a piezo response in the sample surface ($A_{tip\text{-}samp}$, $\phi_{tip\text{-}samp}$). The cantilever in contact with the surface has a resonance defined by the mechanical properties of the cantilever and the stiffness of the tip-sample contact. This resonance can have a high (*Q*) for typical PFM samples that effectively amplifies the piezo signal by a factor of ~*Q* near the resonance. For samples with small piezo coefficients, this is potentially a very important effect and could mean the difference between only noise or a measurable signal. Unfortunately, because the cantilever resonance frequency depends on the tip-sample contact stiffness, the resonance frequency is very unstable. As the tip scans over the sample topography, the stiffness of the mechanical contact ($k_{tip\text{-}samp}$) will typically change significantly. This, in turn, affects the resonance frequency.

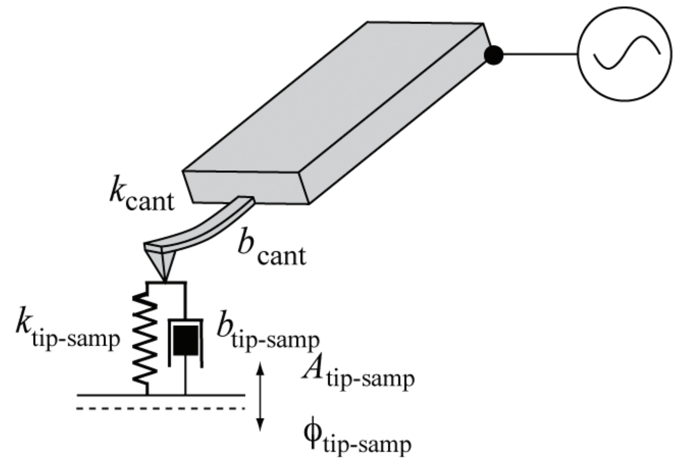

Figure 13: In PFM, the cantilever voltage is modulated, usually at some fixed frequency. This causes the sample to distort at some amplitude and phase. Mediated by the contact mechanics, this drives the tip which, in turn, is monitored by the AFM sensor.

To understand how resonance is affected in PFM, we first describe an "ideal" situation as illustrated in Figure 14. This shows a numerical simulation of the cantilever response using realistic cantilever parameters (Olympus AC240 cantilever with a 320 kHz contact resonant frequency, 2 N/m spring constant) and sample parameters ($d_{33} \approx 100$ pm/V). The noise visible in the PFM amplitude and phase curves were calculated to be the ideal thermal (Brownian motion) noise of a cantilever at typical room temperature (300 K). Here, the domain structure is shown in the middle of the image with purely vertical polarization vectors. The sample is treated as perfectly smooth, meaning that the contact stiffness remains constant as a function of position. The simulation reproduces many of the features present in a real scan where the measured phase reproduces a map of the domain structure, and the amplitude goes to zero at the domain boundaries. This occurs as the tip is being driven by two oppositely oriented domains, each canceling the other since they are 180° out of phase. As discussed below, real-world samples have behaviors that make extracting unambiguous domain maps much more complicated.

The gain in the signal from the *Q*-factor when operating near resonance improves the SNR for the PFM amplitude and the phase. This is illustrated in Figure 15 which shows the same sample as in Figure 14 but now imaged with the cantilever voltage being modulated at the cantilever resonance. This should not come as a surprise; as with many other types of dynamic SPM, oscillating at the cantilever resonance greatly benefits the SNR. However, the experimental conditions shown in Figure 14 are very rare. Usually, the sample will have some roughness. This roughness will lead to position-dependent changes in the contact resonant frequency. The effects of this resonant frequency variation on PFM contrast can easily completely mask the desired PFM signal. Figures 16, 17, and 18 illustrate this.

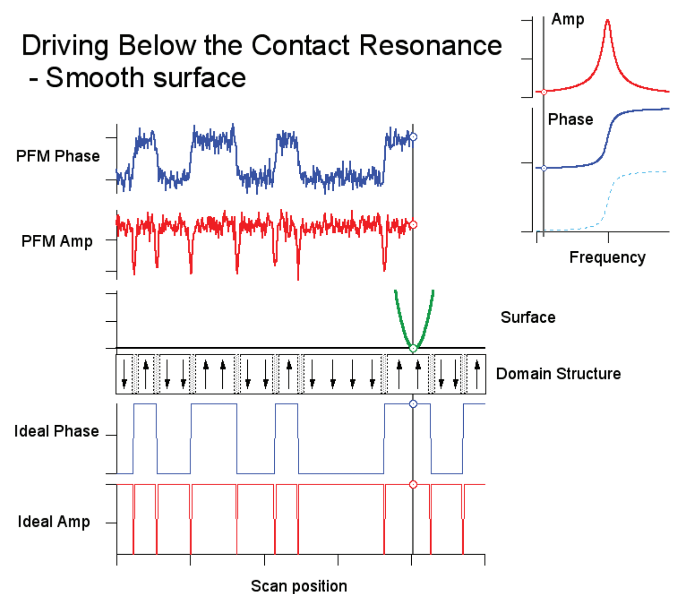

Figure 14: This figure shows the ideal and measured PFM response of an idealized tip (green) scanning over a smooth surface (black line below the "tip"). The domain structure of the ferroelectric sample is shown below the surface where the arrows correspond to the sample polarization direction. The gray hatched regions between the domains are representative of the domain walls. The "ideal phase" (blue, thin curve) and "ideal amp" (red thin curve) show the idealized response of a probe that measures the piezoelectric response over the domains. The measured PFM amplitude (red, thick curve) and phase (blue, thick curve) channels appear above the scanning tip. Because these measurements are made below the resonant frequency where there is no resonance enhancement of the PFM signal, the signal to noise is relatively small for the measured signal.

If we return to our idealized sample and add roughness to the surface, we can see that it modulates the contact resonance. For example, if the tip is on a tall part of the sample, it is in contact

with a relatively compliant part of the sample. Sharp points are, after all, relatively easy to blunt. Because the contact stiffness is small, the contact resonance frequency will drop. If the cantilever is being driven at a fixed frequency, the phase will increase as the resonance moves to lower values. Conversely, if the tip is in a valley, the contact stiffness will be increased, raising the resonant frequency and the phase measured at a fixed frequency will drop. Phase shifts associated with changes in the contact resonance sum with phase shifts due to domain structures of the piezo material. As a consequence, interpretation of the domain structure becomes much more difficult and in many cases, impossible. Figure 16 shows a case where the domains are completely masked by the large phase shifts originating with the moving contact resonance.

Another source of phase shifts can come from irreversible changes to the cantilever itself. PFM is a contact mode technique and therefore can exert large forces on the tip. If the tip fractures or picks up a contaminant, the contact resonance can experience a sudden jump, usually positive, since tip wear tends to blunt the tip. The resonance jumps are typically of the order of a few kHz. This causes large, discontinuous changes in the measured phase. Figures 17 and 18 show PFM data taken on a rough PZT surface. A number of successive tip changes caused the contact resonance to change, resulting in an irreversible change in the overall measured phase. Note that in addition to these jumps, there is significant "roughness" in the phase signals that probably originates with topographic contact resonance crosstalk.

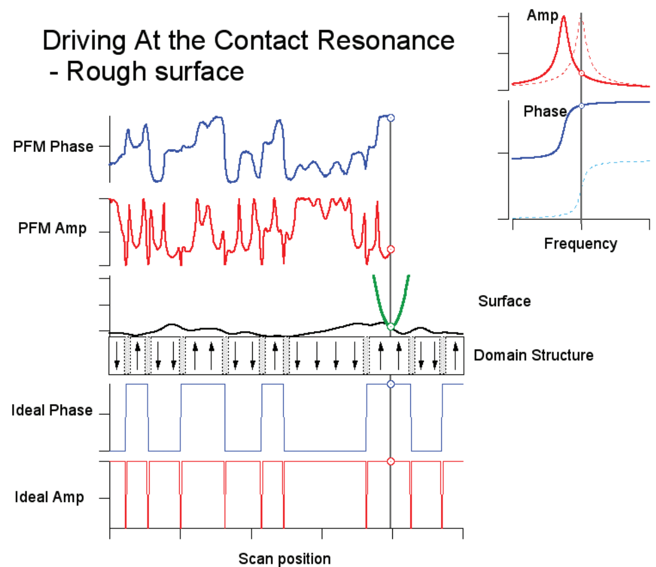

Figure 16: This figure shows a practical limitation of using the contact resonance as the drive frequency. In conventional PFM systems, the contact resonance can change by 10-30 kHz over the course of imaging a rough sample. Typical cantilevers have a full-width half max of 4-10 kHz meaning the phase shift due to the changing contact resonances will easily be near 180° over the scan. The PFM phase shift will be added to the phase of the cantilever contact resonance, yielding a convolution that makes practical interpretation of domain structures very difficult. This is clear in comparing the PFM phase signal to the sample domain structure. In contrast to the off-resonance smooth sample, it is quite difficult to correlate the domain structure with the PFM phase.

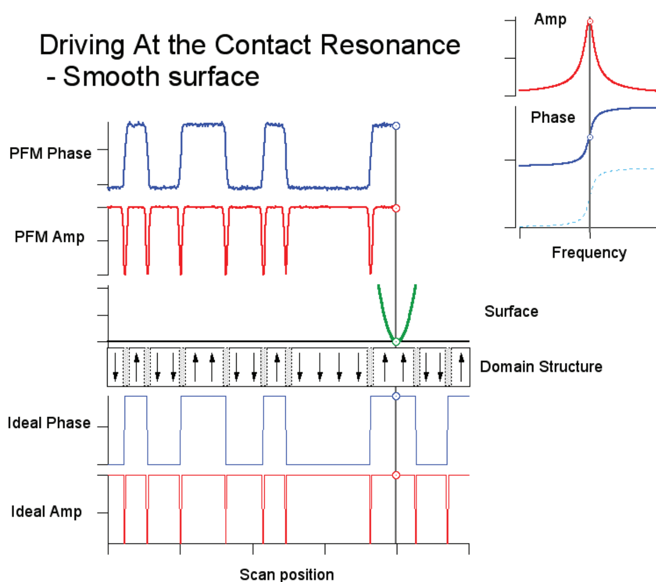

Figure 15: This figure shows the same situation as described in Figure 14, except that here we are using resonance enhancement to boost the small PFM signal. The inset frequency tune in the upper right corner shows the drive frequency. In this case, since the Q-value of the resonance is 100, the SNR of the measured PFM amplitude (red, thick curve) and phase (blue, thick curve) has dramatically improved.

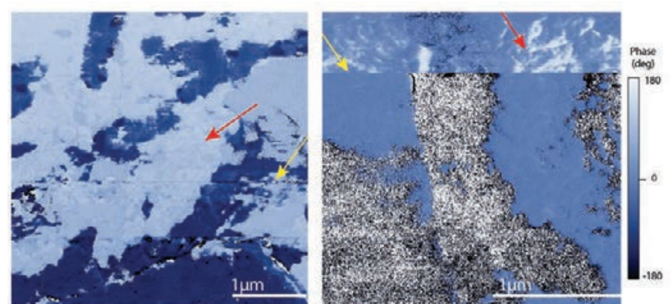

Figure 17 (left): PFM phase channel on a polished PZT sample. The cantilever was driven near the contact resonance to enhance the SNR. There is significant crosstalk between the sample topography and the PFM signal. Red arrows indicate "roughness" where the contact stiffness modulates the phase. In addition to the surface roughness changing the contact resonance and therefore the measured phase, changes in the tip can also cause large phase shifts. The yellow arrows indicate a sudden tip change caused a change in the contact resonance. 4 µm scan (left), 2 µm scan (right).

By avoiding the resonance, the topographic crosstalk on rough samples can be reduced, as shown in Figure 19. When the cantilever is driven well below resonance, the domain structure is reproduced quite accurately. However, this comes at the high price of a poor SNR. In practice, the reduced SNR (see in particular the PFM phase trace) may obviate imaging of a large number of weak piezo materials with conventional PFM.

To summarize the discussion in this section, with conventional PFM imaging and the contact resonance, we are left with the situation where we need to choose between two sub-optimal alternatives:

1. Operate on resonance to benefit from the boosted signal but have complicated artifacts that do not allow unambiguous determination of the sample domain structure, or
2. Avoid resonance to minimize topographic crosstalk, but suffer from the small signals inherent in piezo materials.

In the following sections we discuss new solutions for improving our PFM options with Asylum's PFM and SPM capabilities.

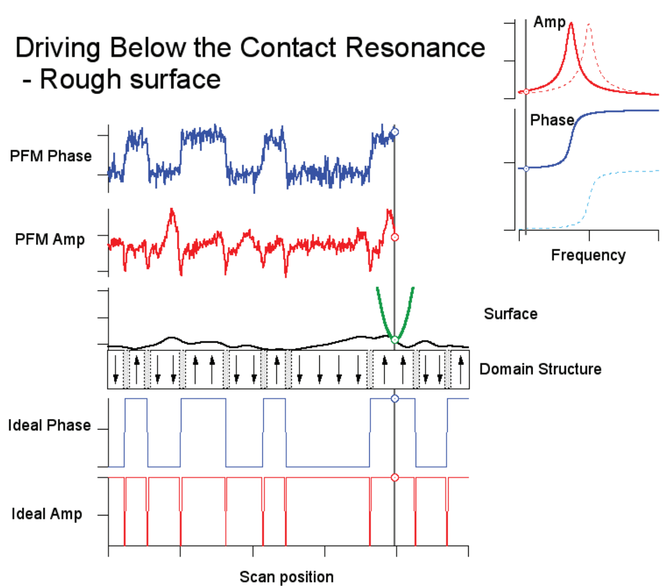

Figure 19: Driving below contact resonance with conventional PFM. Here, the cantilever is driven well below the contact resonant frequency. The effects of surface roughness are minimized, though still visible in the measured PFM amplitude. However, this reduction in crosstalk comes at the high price of severely reduced sensitivity. Thus, for weak piezo materials, this operational mode is undesirable. The improved topographic crosstalk rejection results in an immeasurably small signal with conventional PFM.

Solutions to Limits of Conventional PFM with Asylum's PFM and SPM Capabilities

1. Increasing the Drive Voltage

Perhaps the most obvious option for improving the response of PFM is to simply increase the drive amplitude. The signal is usually proportional to the drive voltage, so increasing the drive voltage by 10x will result in a 10x improvement in the SNR. A more powerful drive amplifier also enables operation at higher frequencies (see below under Emerging Applications for PFM).

Asylum's Piezoresponse Force Module is currently the only commercially-available AFM that enables high voltage PFM measurements. A programmable bias of up to +220 V for the MFP-3D and up to +150 V for the Cypher AFM is applied to the AFM tip using a proprietary high voltage amplifier, cantilever and sample holder. The amplitude of the response measures the local electromechanical activity of the surface while the phase yields information on the polarization direction. High probing voltages can characterize even the weakest piezoelectric sample and insure that you have the ability to switch the polarization of high-coercivity materials. The fully integrated system allows both PFM imaging modes and spectroscopy modes. All PFM imaging and spectroscopy modes are fully integrated with the AFM system software and Piezoresponse Force Module hardware. An easy-to-use PFM menu panel (Figure 20) provides users with point-and-click navigation to the operation they wish to perform. For advanced users, custom panels can by created within the flexible IGOR Pro environment.

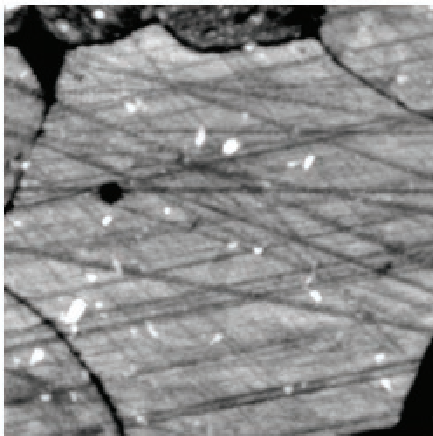

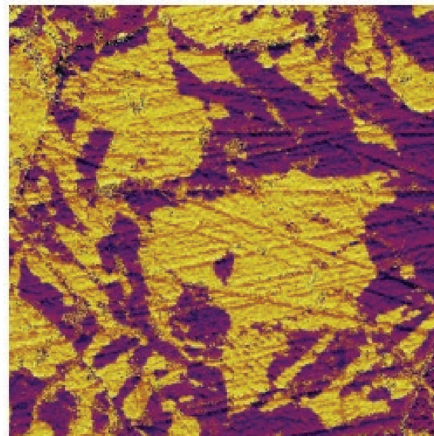

Figure 18 (right) PZT showing crosstalk, 14 µm scan.

Figure 20: MFP-3D Piezo Force Module software menu allows easy point and click navigation.

2. Using Contact Resonance as a PFM Amplifier

Sometimes increasing the SNR by simply increasing the drive voltage is not an option. In some ferroelectric samples, the polarization might be reversed by too large a PFM drive voltage. On others, the sample might actually breakdown, leading to large current flow, sample damage or even destruction. Another effective way to increase the SNR in PFM imaging and other measurements is to make use of the contact resonance. Resonance enhances the signal by the natural gain of the cantilever – by roughly the factor *Q* of the cantilever.

As noted above, driving near the contact resonance at a fixed frequency can sometimes lead to enormous topographic cross-coupling. To avoid this, and to maintain the advantages of resonance, requires that we continually adjust the drive frequency to keep it at the contact resonance. If one can remain on resonance despite changes in the contact resonance frequency, then the artifacts present in the above examples would not be present, while still reaping the resonance amplification.

The most common kind of resonance-tracking feedback loop is called a phase-locked loop (PLL). It utilizes the phase sensitive signal of a lock-in amplifier to maintain the system at a specific phase value, typically 90°. The PLL is generally limited to techniques where the phase and amplitude of the driving force is constant (e.g. the mechanical excitation of a cantilever resonance using an external actuator). This is manifestly not the case in PFM, where the relationship between the phase of the excitation force and driving voltage strongly depends on material properties.[21, 22] The amplitude and phase of the local response are a convolution of material response to the external field and cantilever response to the material-dependent local force, which cannot be separated unambiguously. Figure 21 is an example where, for antiparallel domains, a conventional PLL will actually drive a PFM away from resonance.

3. Dual AC Resonance Tracking (DART)

This patent pending dual-excitation method allows the cantilever to be operated at or near resonance for techniques where conventional PLLs are not stable. Figure 22 shows how DART works. The potential of the conductive cantilever is the sum of two oscillating voltages with frequencies at or near the same resonance. The resulting cantilever deflection is digitized and then sent to two separate lock-in amplifiers, each referenced to one of the drive signals. By measuring the amplitudes at these two frequencies, it is possible to measure changes in the resonance behavior and furthermore, to track the resonant frequency. Specifically, by driving at one frequency below resonance (A1), and another above (A2), A2-A1 gives an error signal that the ARC2™ controller uses to track the resonance frequency changes.[21]

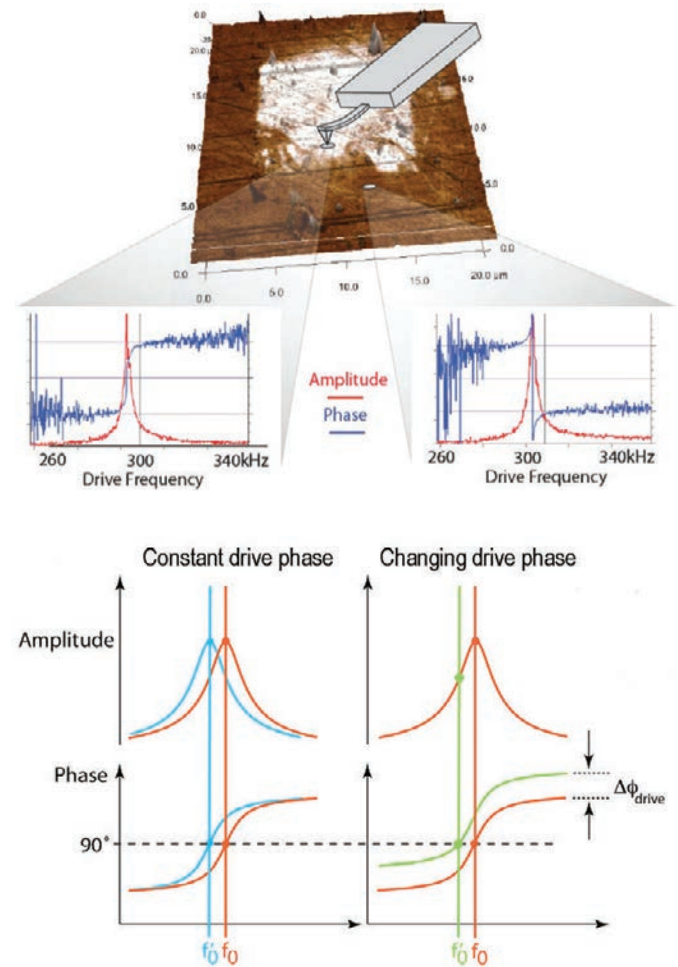

Figure 21: For domains with an antiparallel (180°) orientation, conventional PLLs drive the PFM frequency away from resonance. (Top) Amplitude, red, and phase, blue, cantilever response over antiparallel domains. In the measurement, phase is offset by 180° over anti-parallel domains (see curves on the right). (Bottom) PFM phase signal driving the cantilever off resonance. Note the increased noise in the phase signal away from the resonant frequency. This increased noise would be apparent in an image as well, similar to the PZT image in Figures 17 and 18. Printed with permission (see reference 21).

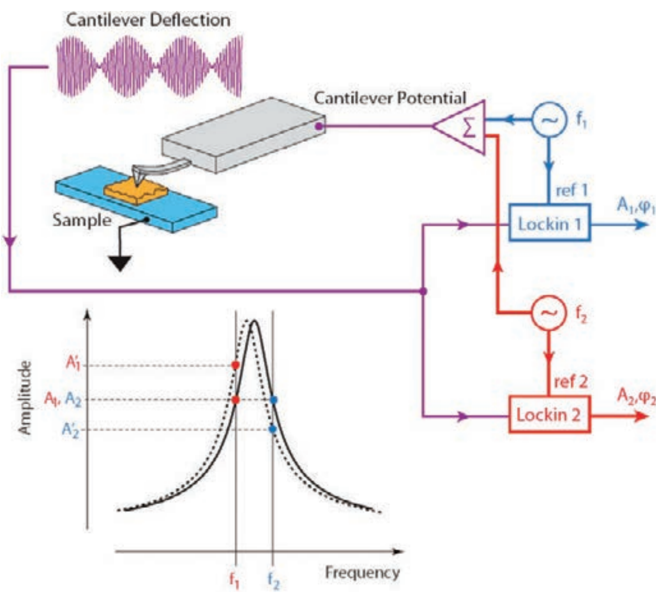

Figure 22: Schematic diagram of Asylum Research's new DART showing a drive phase independent feedback signal. Printed with permission (see reference 21).

DART-PFM studies of polarization switching are illustrated in Figure 23, where the resonant frequency (A), amplitude (B) and phase (C) images of a lithium niobate surface are shown Figure 23(A). The PFM amplitude and phase images show a macroscopic 180° domain wall and two inversion domains which are typical for this material. Higher resolution DART-PFM images of pre-existing domains (D-F) illustrate strong frequency contrast, and nearly constant PFM amplitudes within and outside the domain. In comparison, Figures 23(G-I) are DART-PFM images of domains switched by the application of three 176 V magnitude pulses for ~10 seconds in three adjacent locations. Note the significant change of resonant frequency and the strong amplitude depression in the newly fabricated domain.[21]

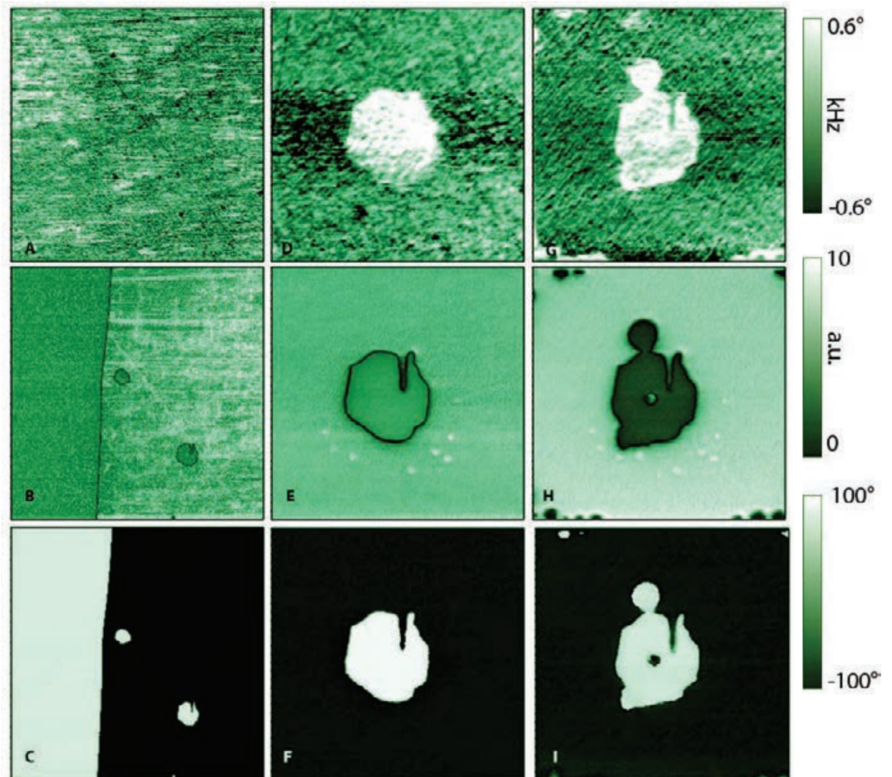

Figure 23: (A), (D), (G) Resonance frequency, (B), (E), (H) piezoresponse amplitude and (C), (F), (I) piezoresponse phase images of antiparallel domains in lithium niobate. Shown are images of the (A)–(C) native domain structure, (D)–(F) an intrinsic domain and (G)–(I) domains switched by ±176 V (locations marked in (E)). The images are obtained at wf = 4 kHz and V_{ac} = 66 V. The frequency images have been flattened to account for minute changes of contact radius from line to line. Reprinted with permission (see reference 21).

Additional DART images of ferroelectric materials are shown in Figures 24 and 25. Figure 24 shows a series of images of PFM on multiferroic $BiFeO_3$ nanofibers. Figure 25 shows a short relaxation study on a sol-gel sample. Regions of the sol-gel PZT were reversed by applying a 15 V bias to the tip. These regions gradually relaxed over a 1.5 hour period. DART allowed stable, reproducible imaging over an extended period of time.

4. Band Excitation (BE)

Band Excitation is a new option that can be utilized with PFM. The technology is exclusively available with Asylum Research SPMs under license from Oak Ridge National Laboratory[23] and has received the R&D 100 award for 2008. The Band Excitation controller and software extend the capabilities of Asylum's MFP-3D and Cypher AFMs to probe local amplitude vs. frequency curves and transfer functions and map local energy dissipation on the nanoscale.

The applicability of SPM for mapping energy transformations and dissipation has previously been limited by the fundamental operation mechanism employed in nearly all conventional SPMs; i.e., the response was measured at a single frequency. Determining dissipation with a single frequency measurement required time-consuming multiple measurements. Simply put, there were more uncertainties than there were measured quantities (see Equations (4) and (5)).[23] BE surmounts this difficulty by detecting responses at all frequencies simultaneously. BE introduces a synthesized digital signal that spans a continuous band of frequencies, and monitors the response within the same frequency band. This allows ~100x

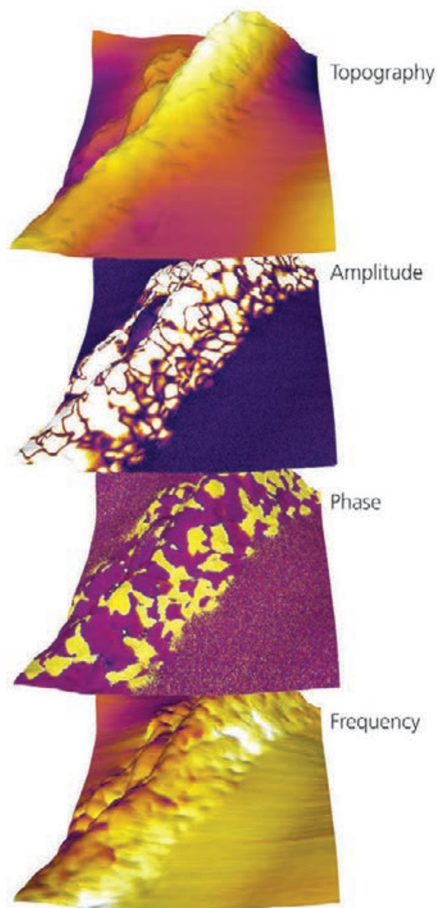

Figure 24: PFM of multiferroic $BiFeO_3$ nanofibers, 1 µm scan. Collaboration with Shuhong Xie, Xiangtan University, China and JiangYu Li, University of Washington.

improvement in data acquisition speed compared to other commercially-available technologies.

The immediate benefit of this approach is that a full response spectrum can be collected (with insignificant [30-50%] decrease in signal to noise ratio) in the amount of time required for obtaining a single pixel in conventional single-frequency SPM. BE allows quantitative mapping of local energy dissipation in materials on the nanoscale.[23] Figure 27 shows an example image of an amyloid fibril (bovine insulin) on mica imaged in water using the BE-PFM technique. The image size 250 nm x 250 nm.

In summary, both DART and BE modes have numerous advantages for PFM measurements:

- SNR is increased by a factor of 100, eliminating crosstalk issues by using, rather than avoiding, resonance.
- Eliminates the problems with PLL stability.
- For BE, data acquisition is improved by ~100x compared to other commercially-available swept frequency technologies.
- Imaging modes and hardware are fully integrated.

Emerging Applications for PFM

1. High Frequency PFM

High-frequency imaging allows for an improved SNR by avoiding 1/f noise. Furthermore, inertial stiffening of the cantilever improves contact conditions. By probing the PFM signal with higher resonances, topographic imaging is performed with a soft cantilever, while PFM is performed with a higher mode where the dynamic stiffness is much greater. This both reduces the electrostatic contribution to the signal and improves the tip-surface electrical contact through effective penetration of the contamination layer. Finally, resonance enhancement using the higher mode amplifies weak PFM signals. It should be noted that in this regime, the response is strongly dependent on the local mechanical contact conditions, and hence, an appropriate frequency tracking method is required to avoid PFM/topography cross-talk, e.g. using DART or BE as described above.

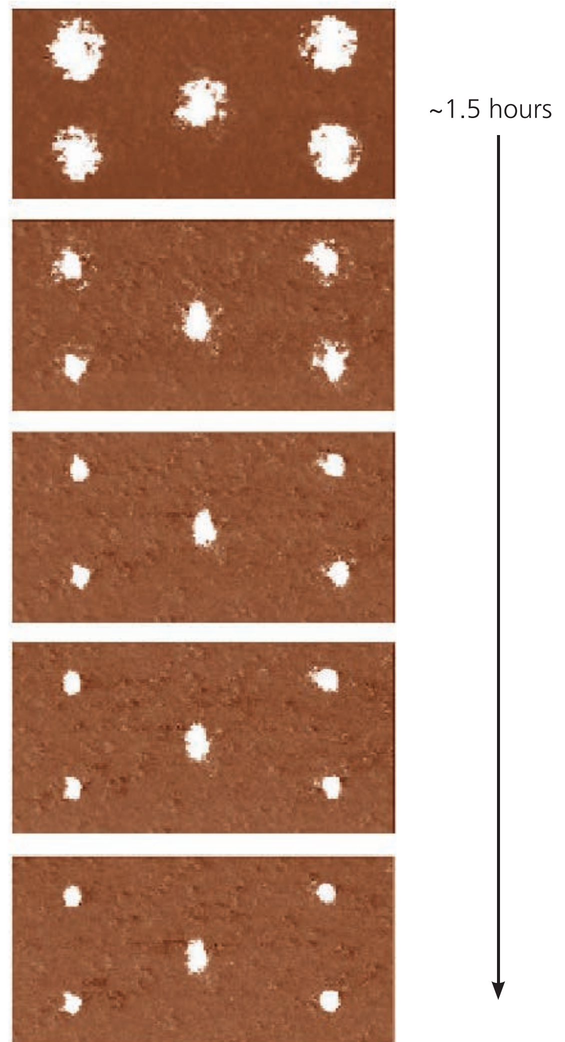

Figure 25: Stable imaging using DART allows relaxation studies. This series of images shows the relaxation of sol-gel taken at different intervals for approximately 1.5 hours. 3.5 µm scan.

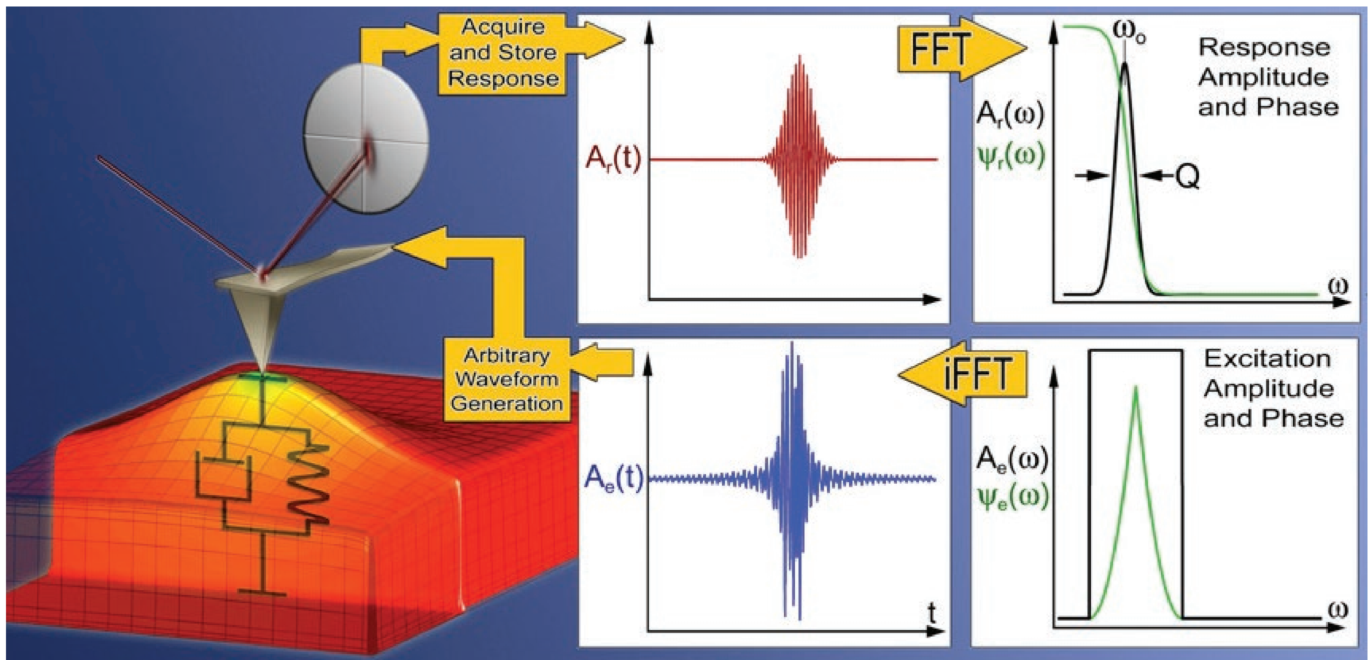

Figure 26: Operational principle of the BE method in SPM. The excitation signal is digitally synthesized to have a predefined amplitude and phase in the given frequency window. The cantilever response is detected and Fourier transformed at each pixel in an image. The ratio of the fast Fourier transform (FFT) of response and excitation signals yields the cantilever response (transfer function). Fitting the response to the simple harmonic oscillator yields amplitude, resonance frequency, and Q-factor, that are plotted to yield 2D images, or used as feedback signals.[23] Reprinted with permission (see reference 23).

The limiting factors for high-frequency PFM include inertial cantilever stiffening, laser spot effects, and the photodiode bandwidth. Inertial stiffening is expected to become a problem for resonances n>4-5, independent of cantilever parameters. This consideration suggests that the use of high-frequency detector electronics, shorter levers with high resonance frequencies, and improved laser focusing will allow the extension of high-frequency PFM imaging to the 10-100 MHz range. Asylum's microscopes allow cut-off at ~2-8 MHz and potentially higher, opening a pathway for high frequency studies of polarization dynamics. Figure 28 illustrates the different information that is revealed by imaging a ceramic PZT material at various frequencies.

2. High-Speed PFM (HSPFM)

HSPFM utilizes high speed data acquisition and sample actuation to significantly enhance imaging speeds by increasing line rates from roughly 1 Hz to well above 100 Hz. The strong amplitude and phase contrast achievable in PFM, as well as the resolution enhancement provided by this contact-mode based method, have allowed 10 nm spatial resolution even at image rates of up to 10 frames per second.[24]

In addition to higher throughput, the primary benefit of this advance is dynamic measurements, for example tracking the evolution of ferroelectric domains during switching, exposure to light, changing temperature, and other effects Figures 29, 30.

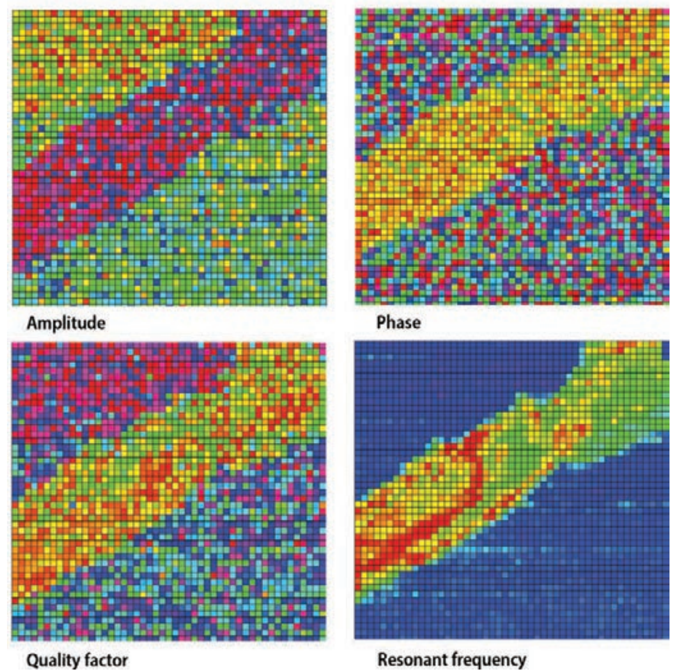

Figure 27: Amyloid fibril (bovine insulin) on mica imaged in water using BE-PFM technique, 250 nm x 250 nm. Image courtesy of G.L. Thompson, V.V. Reukov, A.A. Vertegel, M.P. Nikiforov, Clemson University, Dept. Bioengineering, and S. Jesse, S.V. Kalinin, Oak Ridge National Lab.

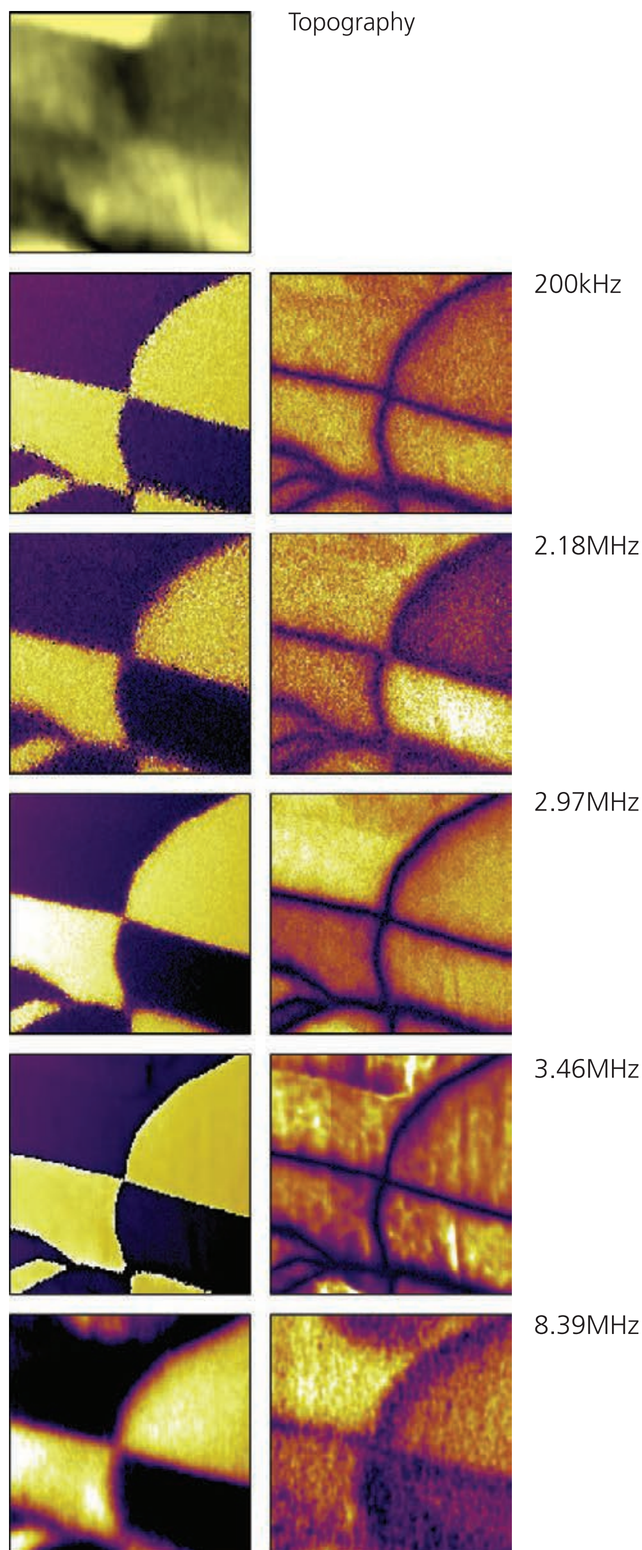

Figure 28: High Frequency PFM using Asylum's fast photodiode on a ceramic PZT sample at different frequencies (phase left, amplitude right) – below first resonance (top row) and at cantilever resonances (all others) using a MikroMasch NSC 35B cantilever. 1 μm scans. Image courtesy of K. Seal, S. Kalinin, S. Jesse, and B. Rodriguez, Center for Nanophase Materials Science, ORNL.

The more general High Speed Scanning Property Mapping (HSSPM) allows rapid measurements of mechanical compliance, electric fields, magnetic fields, friction, etc, with similar benefits for novel dynamic measurements of surfaces.[25]

3. PFM Nanoindenting

For quantitative materials properties measurements, AFMs have a few well-known shortcomings. One is that the shape of the tip is usually ill-defined. Forces between the tip and sample have a strong dependence on this tip shape and, therefore, extracting materials properties such as the Young's modulus are at best problematic. Another issue is that the cantilever geometry means that the motion of the cantilever tip is not well defined. Specifically, when the cantilever deflects, there is motion along the vertical axis (z-axis) that is well defined, but there is also motion parallel to the sample surface. This motion is not well characterized and in most cases is not even measured.

The ability to probe forces and directly image the piezo response of a sample with the Asylum Research MFP NanoIndenter is an emerging application area.[26] The NanoIndenter consists of a flexure with a calibrated spring constant to which diamond tips are mounted. This flexure is attached to the NanoIndenter AFM head and replaces the standard cantilever holder. Displacement of the indenting flexure is performed with a piezo actuator (head) and measured with a patented nanopositioning sensor (NPS™). The force is computed as the product of the spring constant and the measured indenter flexure displacement. This measurement is done by converting the vertical flexure displacement into an optical signal measured at the standard MFP-3D photodetector. Because the quantities of indentation, depth and force are computed based on displacements measured with AFM sensors, the indenter has much better spatial and force resolution than previous systems.

Figure 31 shows an example image of PPLN acquired with the NanoIndenter. Note that the topographic resolution is not as high as it would be with an AFM cantilever tip, as expected given the larger indenter tip. The amplitude and phase channels show clear, high SNR domain structure, similar to the results one would expect with cantilever-based PFM.

Another example of the experiments that can be performed with the combination of the NanoIndenter and PFM imaging is to study the effects of surface stresses on ferroelectric domain structures with quantitative scratch testing as shown in Figure 32. The top image shows the surface topography of PPLN after it has been purposefully scratched with different loading forces using the NanoIndenter tip.

The next image shows the associated phase signal indicative of the domain structure. The domain boundaries have been distorted by the scratches which implies a lattice change which, in turn, has affected the local polarizability. The final figure in this sequence shows a higher resolution scan where the phase has been overlaid onto the rendered topography, showing a close-up of the distortion in the domain structure.

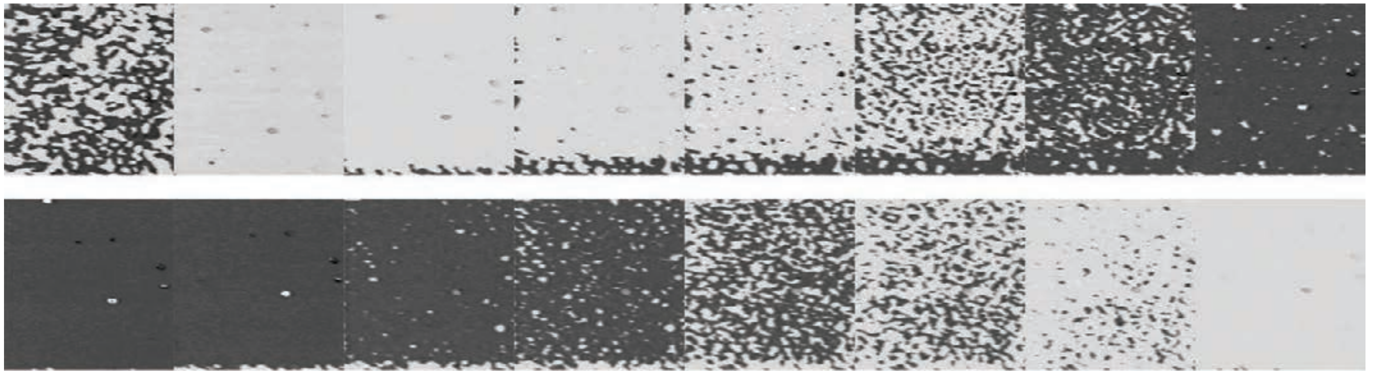

Figure 29: This image sequence (left to right, top to bottom) is excerpted from a movie of 244 consecutive High Speed PFM images (4 µm scans) depicting in situ ferroelectric memory switching. For the first half of the movie, the tip is biased with a positive DC offset throughout the measurements. By monitoring the phase of the piezoresponse, this allows direct nanoscale observation of ferroelectric poling, in this case from white to black contrast (a 180 degree polarization reversal). The second half of the movie is then obtained with a continuous negative DC bias, causing a black to white contrast shift. The switching mechanism is clearly nucleation dominated for this sample and experimental conditions. Each image is acquired in just 6 seconds. The PZT film is courtesy of R. Ramesh, UC Berkeley, and the HSPFM measurements were performed by N. Polomoff, HueyAFMLabs, UConn.

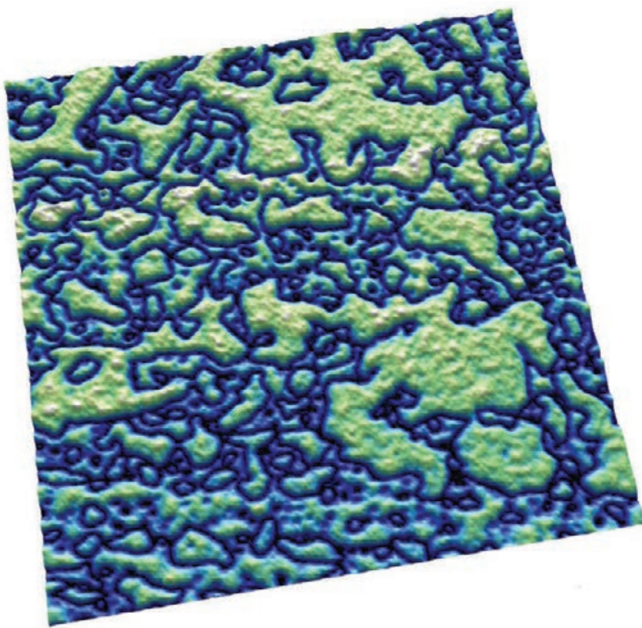

Figure 30: (001) domains in a PZT thin film, 3.8 µm scan. Image courtesy N. Polomoff and B.D. Huey, University of Connecticut Institute of Materials Science. Sample courtesy R. Ramesh, UC Berkeley.

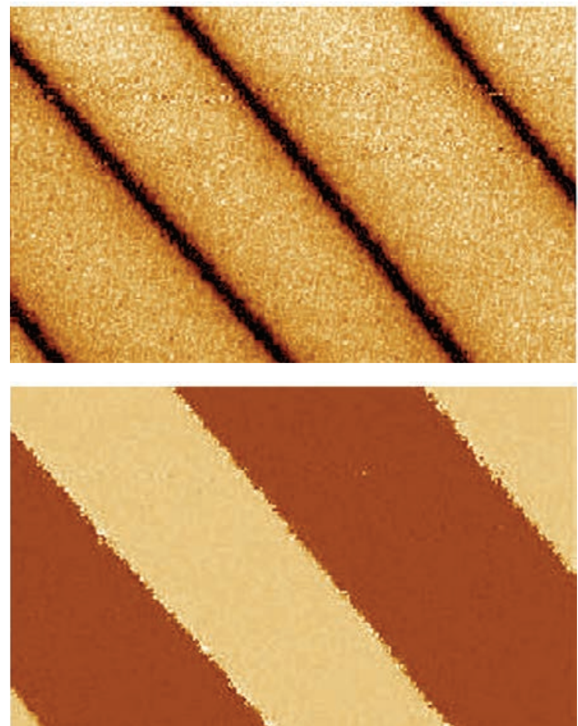

Figure 31: PPLN amplitude (top) and phase image (bottom) acquired with the MFP NanoIndenter, 50 µm scan.

Figure 32: Surface topography of PPLN after it has been purposefully scratched with different loading forces using the NanoIndenter, 10 μm scan (top and middle images). 1 μm scan (bottom).

4. Biological Applications

PFM allows organic and mineral components of biological systems to be differentiated and provides information on materials microstructure and local properties. The use of vector PFM may also enable protein orientation to be determined in real space, for example, the internal structure and orientation of protein microfibrils with a spatial resolution of several nanometers in human tooth enamel. Additional progress will bring understanding of electromechanical coupling at the nanometer level, establish the role of surface defects on polarization switching (Landauer paradox), and probe nanoscale polarization dynamics in phase-ordered materials and unusual polarization states. In biosystems, PFM can also potentially open pathways for studies of electrophysiology at the cellular and molecular levels, for example, signal propagation in neurons. Ultimately, on the molecular level, PFM may allow reactions and energy transformation pathways to be understood, and become an enabling component to understanding molecular electromechanical machines. Recently, PFM performed on biomolecules has demonstrated electromechanical behavior in lysozyme polymers, bacteriorhodopsin, and connective tissue.[21, 27] Figure 33 shows an example of vertical PFM height and phase images of collagen fibers. PFM has also recently been performed on biological systems such as cells as shown in Figure 34.[28] This image shows a zoom of a red blood cell with the PFM phase channel painted on top to show piezo response.

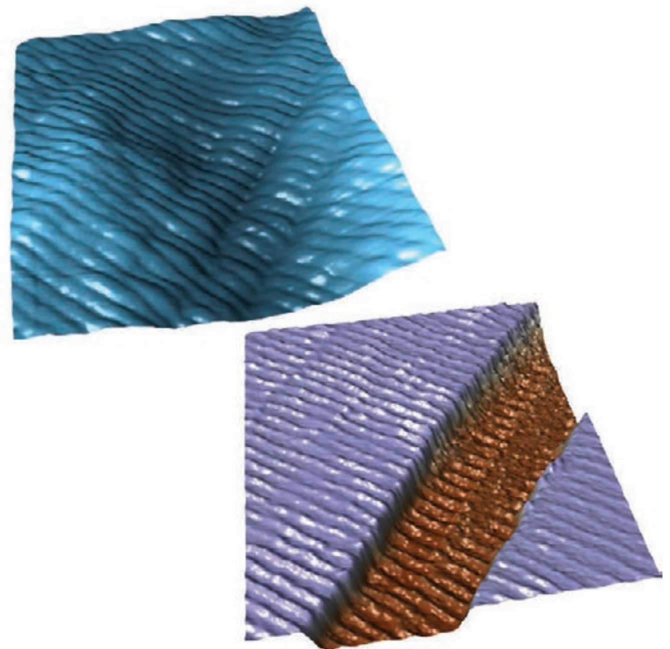

Figure 33: Topographic (top) and PFM phase (bottom) images of collagen fibers, 1.4 μm scan. Image courtesy D. Wu and A. Gruverman, UNL. Sample courtesy G. Fantner.

Applications of Piezoresponse Force Microscopy

Fundamental Materials Science

- Domains
- Phase Transitions and Critical Phenomena
- Size Effects
- Nucleation Dynamics
- Multiferroics
- Ferroelectric Polymers
- Liquid Crystals
- Composites
- Relaxor Ferroelectrics

Piezoelectric Materials

- Micro ElectroMechanical Systems (MEMS)
- Sensors and Actuators
- Energy Storage and Harvesting
- RF Filters and Switches
- Sonar
- Balance and Frequency Standards
- Giant k Dielectrics
- Capacitors

Ferroelectric Materials

- Domain Engineering
- Non-volatile Memory
- Data Storage Devices
- Domain Energetics and Dynamics

Bio-electromechanics

- Cardiac
- Auditory
- Cell Signaling
- Structural Electromechanics
- Biosensors

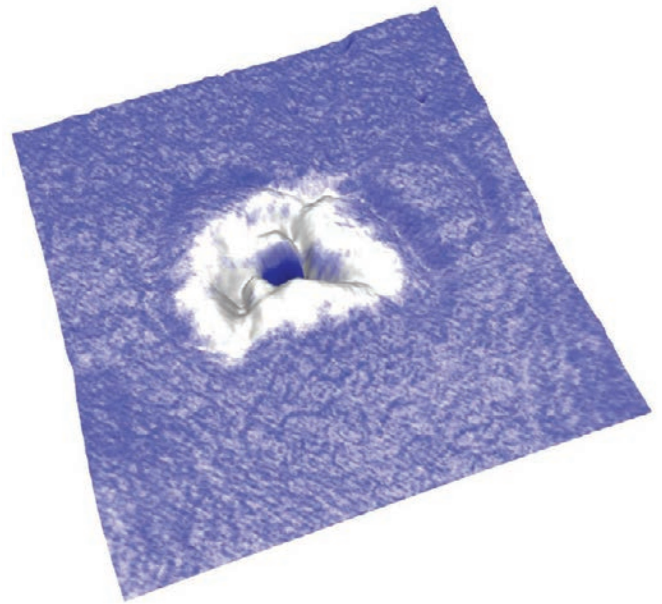

Figure 34: Zoom of the top surface of a red blood cell. The surface shape was rendered to show the topography while the phase channel is overlaid on top to show piezo response. A small sub-micron region on top (white) of the cell exhibited a much different piezo response than the surrounding cell surface. 2 µm scan. Image courtesy of B. Rodriguez and S. Kalinin, ORNL.

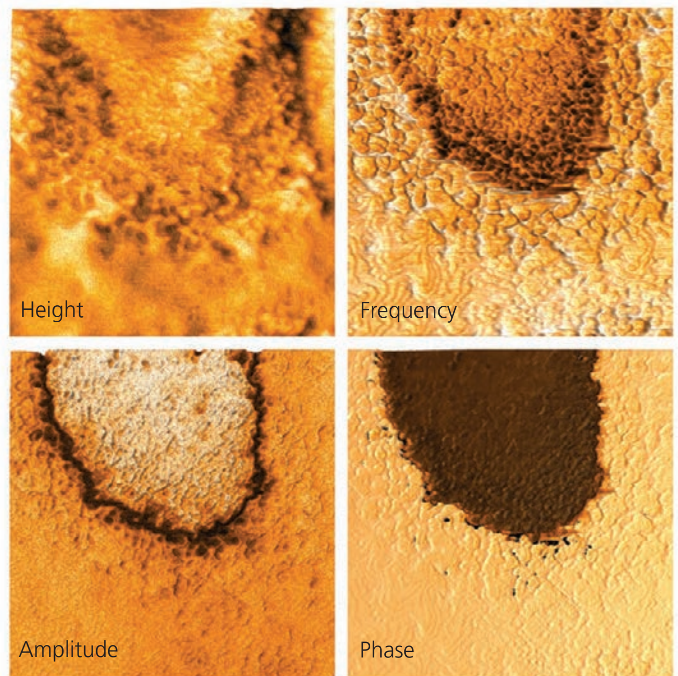

Figure 35: DART image of C-domains in lead titanate thin film, 5 µm scan. Image courtesy D. Wu and A. Gruverman, UNL.

Conclusion

Characterizing electromechanical responses in a variety of materials will be crucial for understanding and improving technologies ranging from bioscience to energy production. Scanning probe microscopy has emerged as a universal tool for probing such structures and functionality at the nanometer scale. Asylum's Piezoresponse Force Microscopy capabilities now allow characterization of an endless variety of materials and devices that previously could not be measured using conventional piezoresponse force microscopy. Research with this new tool will enable new advancements in many disciplines from biology to semiconductors, while yielding improvements for ongoing work in diverse areas from data storage devices and molecular machines to improved materials for renewable energy.

References

1. S.V. Kalinin, B.J. Rodriguez, S. Jesse, B.Mirman, E. Karapetian, E.A. Eliseev, A.N. Morozovska, *Annu. Rev. Mat. Sci.* **37**, 189 (2007).
2. K. Uchino, *Ferroelectric Devices*. Marcel Dekker, New York (2000).
3. J. Scott. 2000. *Ferroelectric Memories*. Springer Verlag, Berlin (2006).
4. S. Jesse et al., *Rev. Sci Inst.* **77**, 073702 (2006).
5. L.M. Eng, H-J. Güntherodt, G.A. Schneider, U. Köpke, J. Muñoz Saldaña, *App. Phys. Lett.* **74**, 233-35 (1999).
6. S.V. Kalinin, B.J. Rodriguez, S. Jesse, S. Shin, A.P. Baddorf, P. Gupta, H. Jain, D.B. Williams, A. Gruverman, *Microscopy and Microanalysis* **12**, 206-20 (2006).
7. A. Verdaguer, G.M. Sacha, H. Bluhm, M. Salmeron,*Chem. Rev.* **106**:1478-510 (2006).
8. G.M. Sacha, A. Verdaguer, M. Salmeron, *J. Phys. Chem. B* **110**, 14870-73 (2006).
9. E.A. Eliseev, Sergei V. Kalinin, S. Jesse, S.L. Bravina, and A.N. Morozovska, *J. Appl. Phys.* **102**, 014109 (2007).
10. S. Jesse, A.P. Baddorf, S.V. Kalinin, *Nanotechnology* **17**, 1615 (2006).
11. L.M. Eng, H.J. Güntherodt, G. Roseman, A. Skliar, O. Oron, M. Katz, and D. Eger, *J. Appl. Phys.* **83**, 5973 (1998).
12. L.M. Eng, H.J. Güntherodt, G.A. Schneider, U. Kopke, and J. Muñoz Saldaña, *Appl. Phys. Lett.* **74**, 233 (1999).
13. M. Abplanalp, L.M. Eng, and P. Günter, *Appl. Phys. A: Mater. Sci. Process.* **66A**, S231 (1998).
14. L.M. Eng, M. Abplanalp, and P. Günter, *Appl. Phys. A: Mater. Sci. Process*. **66A**, S679 (1998).
15. A. Roelofs, U. Bottger, R. Waser, F. Schlaphof, S. Trogisch, and L.M. Eng, *Appl. Phys. Lett.* **77**, 3444 (2000).
16. S. Jess, H. Lee, S. Kalinin, *Rev. Sci. Instr.*, **77**, 073702 (2006).
17. S. Jesse, B. Rodriguez, S. Choudhury, A. Baddorf, I. Vrejoiu, D. Hesse, M. Alexe, E. Eliseev, A. Morozovska, J. Zhang, L. Chen, S. Kalinin, *Nature Materials* **7**, 209 - 215 (2008).
18. P. Frederix, M.R Gullo, T. Akiyama, A. Tonin, N.F. de Rooij, U. Staufer, and A. Engel, *Nanotechnology* **16**, 997–1005 (2005).
19. J.E. Sader, *J. Appl. Phys*. **84**, 64 (1998).
20. R. García and R. Pérez, *Surf. Sci. Reports* **47**, 197 (2002).
21. B.J. Rodriguez, C. Callahan, S. Kalinin, R. Proksch, *Nanotechnology* **18**, 475504 (2007).
22. S. Kalinin, S. Jesse, R. Proksch, *R&D Magazine* (Sept. 2008).
23. S. Jesse, S. Kalinin, R. Proksch, A.P. Baddorf, B.J. Rodriguez, *Nanotechnology* **18**, 435503 (2007).
24. R. Nath, Y.H. Chiu, N. Polomoff, R. Ramesh, B.D. Huey, *App. Phys. Lett.* **93**, 072905 (2008).
25. B.D. Huey, A*nnual Reviews of Materials Research,* **37**, 351-85 (2007).
26. A. Rar, G.M. Pharr, W.C. Oliver, E. Karapetian, S. Kalinin, *JMR*, **23** No. 3, 552-556 (2006).
27. S. Kalinin, B.J. Rodriguez, S. Jesse, K. Seal, R. Proksch, S. Hohlbauch, *Nanotechnology* **18**, 424020 (2007).
28. B. Rodriguez, S. Kalinin, S. Jesse, G. Thompson, A. Vertegel, S. Hohlbauch, R. Proksch, *Microscopy Today*, (Jan. 2008).

Additional Material

Although not cited in the application note text, these references may be used for additional reading of the background, theory and applications of PFM.

1. A.E. Giannakopoulos and S. Suresh, *Acta Mater.* **47**, 2153 (1999).
2. W. Chen and H. Ding, *Acta Mech. Solidi. Sin.* **12**, 114 (1999).
3. E. Karapetian, I. Sevostianov, and M. Kachanov, *Philos. Mag. B* **80**, 331 (2000).
4. S.V. Kalinin, E. Karapetian, and M. Kachanov, *Phys. Rev. B* **70**, 184101 (2004).
5. E. Karapetian, M. Kachanov, and S.V. Kalinin, *Philos. Mag.* **85**, 1017 (2005).
6. F. Felten, G.A. Schneider, J. Muñoz Saldaña, and S.V. Kalinin, *J. Appl. Phys.* **96**, 563 (2004).
7. D.A. Scrymgeour and V. Gopalan, *Phys. Rev. B* **72**, 024103 (2005).
8. S.V. Kalinin, E.A. Eliseev, and A.N. Morozovska, *App. Phys. Lett.* **88**, 232904 (2006).

9. E.A. Eliseev, S.V. Kalinin, S. Jesse, S.L. Bravina, and A.M. Morozovska, *Cond-mat*/0607543.

10. A.N. Morozovska, S.L. Bravina, E.A. Eliseev, and S.V. Kalinin, *Cond-mat*/0608289.

11. S.V. Kalinin, S. Jesse, B.J. Rodriguez, J. Shin, A.P. Baddorf, H.N. Lee, A. Borisevich, and S.J. Pennycook, *Nanotechnology* **17**, 3400 (2006).

12. S. Jesse, S.V. Kalinin, B.J. Rodriguez, E.A. Eliseev, and A.N. Morozovska, submitted.

13. *"Nanoscale Phenomena in Ferroelectric Thin Films"* edited by Seungbum Hong (Springer-Verlag New York, LLC, 2004).

14. A.Gruverman, "*Ferroelectric Nanodomains*," in *Encyclopedia of Nanoscience and Nanotechnology*, edited by H. S. Nalwa (American Scientific Publishers, Los Angeles, 2004), **3**, pp. 359-375.

15. "*Nanocrystalline multiferroic* $BiFeO_3$ *ultrafine fibers by sol-gel based electrospinning*", S. H. Xie e.t al. *Applied Physics Letters*, **93**, 222904 (2008).

16. "*Local bias-induced phase transitions*", S. Kalinin, et. al., *Materials Today*, **11** no 11, 2008.

17. Invited Papers from the International Symposium on Piezoresponse Force Microscopy and Nanoscale Phenomena in Polar Materials, Aveiro, Portugal, 2009.

Comprehensive Material

These references provide key papers and comprehensive reviews on PFM:

1. S.V. Kalinin and A. Gruverman (Eds), "*Scanning Probe Microscopy of Electrical and Electromechanical Phenomena at the Nanoscale,*" (Springer, 2006).

2. M. Alexe and A. Gruverman (Eds), "*Ferroelectrics at Nanoscale: Scanning Probe Microscopy Approach,*" (Springer, 2004).

3. A. Gruverman, O. Auciello and H. Tokumoto, *Ann. Rev. of Mat. Science* **28**, 101-124 (1998).

Glossary

Band Excitation
A scanning technique whereby the cantilever is excited and the response is recorded over a band of frequencies simultaneously rather than at a single frequency as in conventional SPM. This allows very rapid data acquisition and enables the direct measurement of energy dissipation through the determination of the Q-factor of the cantilever.

Electromechanical Coupling
The mechanical response to an applied electrical stimulus and the electrical response to an applied mechanical stimulus.

Domain Nucleation
The event of polarization reversal when an oppositely polarized domain is formed in a ferroelectric material.

Dual AC Resonance Tracking (DART)
A scanning technique used in PFM that allows dual excitation of the cantilever to independently measure both the amplitude and resonance frequency of the cantilever, improving spatial resolution and sensitivity. Overcomes limitations of traditional Phase-Locked Loops used in conventional SPM.

Ferroelectric Polarization
A spontaneous dipole moment existing due to the distortion of a crystal lattice that can be switched between two or more stable states by the application of electrical or mechanical stress.

Landauer Paradox
The electric fields required to induce polarization reversal correspond to unrealistically high values for the activation energy for domain nucleation.

Lateral PFM
A PFM technique where the in-plane component of polarization is detected as lateral motion of the cantilever due to bias-induced surface shearing.

Nucleation
The onset of a phase transition or chemical reaction in which a nanoscale region of a new phase forms, e.g., a bubble during boiling of a liquid or a crystal from a liquid.

Phase-Locked Loop (PLL)
In AFM imaging, the PLL measures the phase lag between excitation and response signals as the error signal for a feedback loop that maintains the cantilever phase at a constant value (typically 90°) at resonance by adjusting the frequency of the excitation signal in order to maintain precise control of tip-surface interactions.

Piezoresponse Force Microscopy (PFM)
Scanning probe technique based on the detection of the electromechanical response of a material to an applied electrical bias.

Piezoelectric Surface
A 3D plot depicting the piezoresponse as a function of the angle between the direction of the applied field and the measurement axis.

Q-factor
Typically referred to as the "Q-factor of the cantilever," this is a dimensionless quantity inversely dependent on the cantilever energy dissipation. Typical values of Q range from ten to several hundred.

Resonant Frequency
Typically referred to as the "resonant frequency of the cantilever," it is the natural frequency at which the cantilever is oscillated to achieve maximum amplitude.

Switching Spectroscopy Mapping
A quantitative measurement that reveals local switching characteristics for real-space imaging of imprint, coercive bias, remanent and saturation responses, and domain nucleation voltage on the nanoscale.

Vector PFM
The real space reconstruction of polarization orientation from three components of piezoresponse, vertical PFM and at least two orthogonal lateral PFM.

Vertical PFM (VPFM)
Out-of-plane polarization is measured by recording the tip-deflection signal at the frequency of modulation.

Additional PFM Image Examples

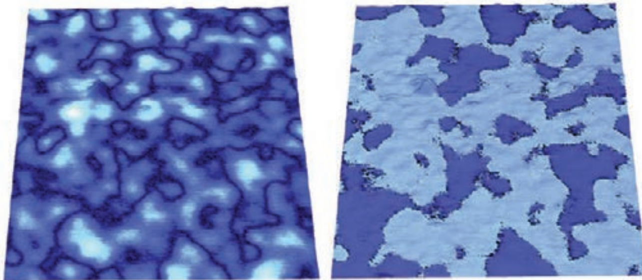

Figure 36: PFM amplitude overlaid on AFM topography (left), and phase overlaid on topography (right) of 1 μm thick PZT film with 50 nm Pt capacitor electrode. A bias was applied between the bottom and top electrodes and the tip was electrically isolated. Taken at a frequency of ~1 MHz, 5 μm scan. Image courtesy of K. Seal, S. Kalinin, S. Jesse, ORNL, and P. Bintachitt, S. Trolier-McKinstry, Pennsylvania State University.

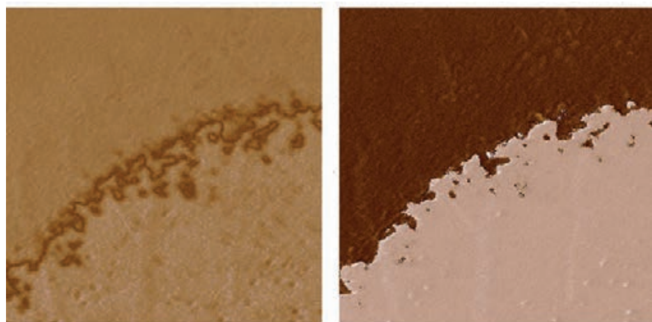

Figure 37: DART image of lead titanate showing domains, amplitude (left) and phase (right), 4 μm scan.

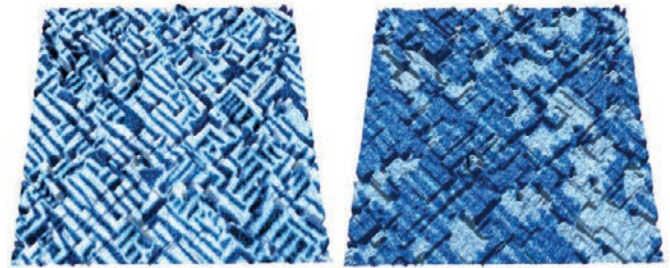

Figure 38: PFM amplitude overlaid on topography (left) and PFM phase overlaid on topography (right) of in-plane images of 50 nm BFO/LMSO/STO(001), V_{ac} = 2V, f = 25 kHz. The in-plane images show stripe-like domains, 5 μm scan. Image courtesy of N. Balke, Department of Materials Science and Engineering, University of California, Berkeley.

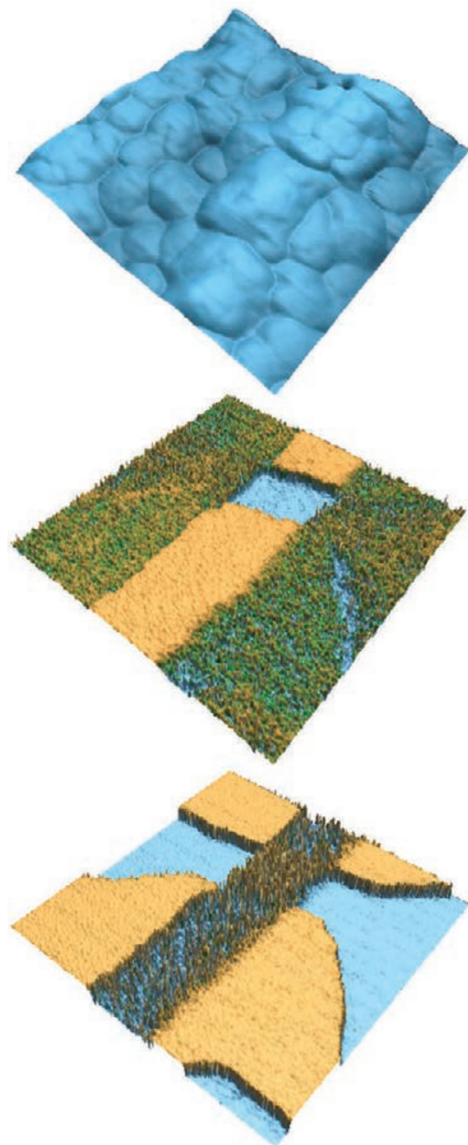

Figure 39: Topography (top), lateral PFM phase (center), and vertical PFM phase (bottom) images of lead titanate film, 3 μm scan. Images courtesy A. Gruverman and D. Wu, UNL. Sample courtesy H. Funakubo.

Visit **www.AsylumResearch.com** to learn more

The foregoing application note is copyrighted by Oxford Instruments Asylum Research, Inc. Oxford Instruments Asylum Research, Inc. does not intend the application note or any part thereof to form part of any order or contract or regarded as a representation relating to the products or service concerned, but it may, with acknowledgement to Oxford Instruments Asylum Research, Inc., be used, applied or reproduced for any purpose. Oxford Instruments Asylum Research, Inc. reserves the right to alter, without notice the specification, design or conditions of supply of any product or service. Application Note 10 – 6/2014.

The Business of Science®

6310 Hollister Avenue
Santa Barbara, CA 93117
Voice +1 (805) 696-6466
Toll free +1 (888) 472-2795
Fax +1 (805) 696-6444

www.AsylumResearch.com
info@AsylumResearch.com
sales@AsylumResearch.com